NASA TN D-983

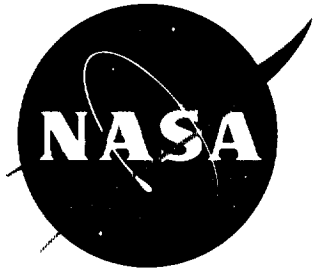

TECHNICAL NOTE

D-983

LOW SUBSONIC PRESSURE DISTRIBUTIONS ON THREE RIGID WINGS SIMULATING PARAGLIDERS WITH VARIED CANOPY CURVATURE AND LEADING-EDGE SWEEP

By Paul G. Fournier and B. Ann Bell

Langley Research Center
Langley Air Force Base, Va.

NATIONAL AERONAUTICS AND SPACE ADMINISTRATION
WASHINGTON November 1961

NATIONAL AERONAUTICS AND SPACE ADMINISTRATION

TECHNICAL NOTE D-983

LOW SUBSONIC PRESSURE DISTRIBUTIONS ON THREE RIGID WINGS SIMULATING PARAGLIDERS WITH VARIED CANOPY CURVATURE AND LEADING-EDGE SWEEP

By Paul G. Fournier and B. Ann Bell

SUMMARY

An investigation has been made in the Langley 7- by 10-foot transonic tunnel to determine the subsonic pressure distribution of three paraglider models through an angle-of-attack range from 0° to 74°. Three rigid metal models simulated a 45° basic flat planform paraglider with leading-edge sweep angles of 61.6°, 52.5°, and 48.6°. These configurations resulted in one-half-circle, one-third-circle, and one-quarter-circle semispan trailing-edge curvature when viewed from downstream. The results of the investigation are presented as curves of chordwise pressure distributions at four spanwise locations.

INTRODUCTION

The Langley Research Center is making studies of the performance, stability, and control characteristics of paragliders at subsonic, transonic, and supersonic speeds. Some preliminary work on the paraglider concept is presented in references 1, 2, and 3.

Increasing interest in the paraglider for applications such as booster recovery and terminal recovery of space capsules has necessitated detailed load distribution data over a range of Mach numbers. Observations of paraglider models in previous investigations have shown that the canopy shape could be closely represented by portions of a conical surface. With this assumption, rigid metal pressure distribution models of varying curvature were constructed (one-half-circle, one-third-circle, and one-quarter-circle trailing edges when viewed from downstream) and tested over a Mach number range from low subsonic to high supersonic speeds.

The present paper presents results of the investigation at low subsonic speeds, in the angle-of-attack range from 0° to 74°. Some discussion on the applicability of the data and a few comments on the general characteristics of the data are included.

SYMBOLS

b	span
C_p	pressure coefficient, $\frac{p_l - p}{q}$
c	local projected chord
p	free-stream static pressure, lb/sq ft
p_l	local pressure, lb/sq ft
q	dynamic pressure, $\frac{1}{2}\rho V^2$, lb/sq ft
V	free-stream velocity, ft/sec
x	distance along keel
z	distance above reference plane
α	nominal keel angle of attack, deg
ρ	density, slugs/cu ft

DESCRIPTION OF MODEL

The pressure distributions were obtained on three 1/10-inch-thick metal and plastic models constructed to simulate a range of conical shapes that the paraglider might assume in flight. The models had a 45° sweep basic flat planform (area of 1 square foot) leading-edge sweep of 61.6°, 52.5°, and 48.6° resulting in one-half-circle, one-third-circle, and one-quarter-circle semispan trailing-edge curvature when viewed from downstream. Photographs of the models are presented in figures 1 and 2.

The difference in curvature was accomplished by development of the panels of each model around a circular cone. (See fig. 3.) The resulting models with panels, one-half of a conical surface, one-third of a conical surface, and one-fourth of a conical surface are designated as models 1, 2, and 3, respectively. Geometric characteristics of all three models are presented in figure 4.

The right and left panels for each model were welded to a hollow center keel which carried small pressure tubes to the wing. The right panel had the lower-surface pressure orifices (including the leading edge and trailing edge) and the left panel had the upper-surface pressure orifices. The fraction of local projected chord location of the orifices at each spanwise station are presented in figure 5. In addition the orifice locations are given vertically above and below the keel reference plane and horizontally with respect to the paraglider keel.

L 1 7 5 7 Plastic leading edges of approximately 3/8-inch diameter were cast to each model. An auxiliary strut extended below the reference plane of the models. (See figs. 1 and 2.) Wires were attached from the strut to the leading edge of the models to reduce the flexure of the paraglider panels. It is felt that the wire and strut had little or no measurable effect on these pressure data.

APPARATUS, TEST, AND CORRECTIONS

The sting-support models were tested in the Langley 7- by 10-foot transonic tunnel at a dynamic pressure of approximately 60 pounds per square foot, which corresponds to an airspeed of about 135 knots. Reynolds number for this airspeed based on the keel length was approximately 1.7×10^6.

The angles of attack have not been corrected due to loads on the model; however, it was estimated that the maximum correction would be about 0.1° or 0.2°.

PRESENTATION OF DATA

Data on the three paraglider models are presented as plots of pressure coefficient C_p against fraction of local chord projected to the plane of the leading edge and keel and are presented in figures 6 to 8. A short discussion on the applicability of the pressure data are presented as well as a few comments on the general characteristics of the data.

It should be pointed out that the pressure data shown at the low angles of attack for these rigid paraglider models will result in negative lift values on all stations. These data at low angles of attack, however, are somewhat academic and not applicable to paragliders since the assumed conical shape will not result with negative lift of the membrane. However, they are useful for rigid conical wings.

Paragliders now being considered for booster and space-capsule application have either large inflatable keel and leading edges or small metal tube keel and leading edges. It is believed that these data will more closely simulate the loads on rigid leading-edge and keel configurations of small diameter.

The inboard pressure-distribution curves for these paraglider models at moderate angles of attack are somewhat similar to conventional flat rigid lifting surfaces in that large peak pressures occur near the leading edge followed by a large adverse pressure gradient. However, these peak pressures were not obtained on the outboard stations. A comparison of the pressure data at the various spanwise stations showed a loss of loading near the tip. The decrease in spanwise loading was less for the paraglider model with the least amount of curvature (i.e., the flattest). These effects might be expected from considerations of the spanwise angle-of-attack variations shown in figure 5.

L 1 7 5 7

CONCLUDING REMARKS

In general, the overall local distribution characteristics shown in the present paper are similar to those obtained on flat rigid triangular wings, with large peak pressures occurring near the leading edge at moderate angles of attack followed by a large adverse pressure gradient. Also, as expected on triangular wings, these data indicate a loss in loading towards the tip.

Langley Research Center,
National Aeronautics and Space Administration,
Langley Air Force Base, Va., September 11, 1961.

REFERENCES

1. Rogallo, F. M., and Lowry, J. G.: Flexible Reentry Gliders. Preprint No. 175C, Soc. Automotive Eng., Apr. 1960.

2. Rogallo, Francis M., Lowry, John G., Croom, Delwin R., and Taylor, Robert T.: Preliminary Investigation of a Paraglider. NASA TN D-443, 1960.

3. Naeseth, Rodger L.: An Exploratory Study of a Parawing as a High-Lift Device for Aircraft. NASA TN D-629, 1960.

(a) Side view. L-61-1732

Figure 1.- Typical model mounted in the Langley 7- by 10-foot transonic tunnel.

(b) One-quarter front view. L-61-1731

Figure 1.- Concluded.

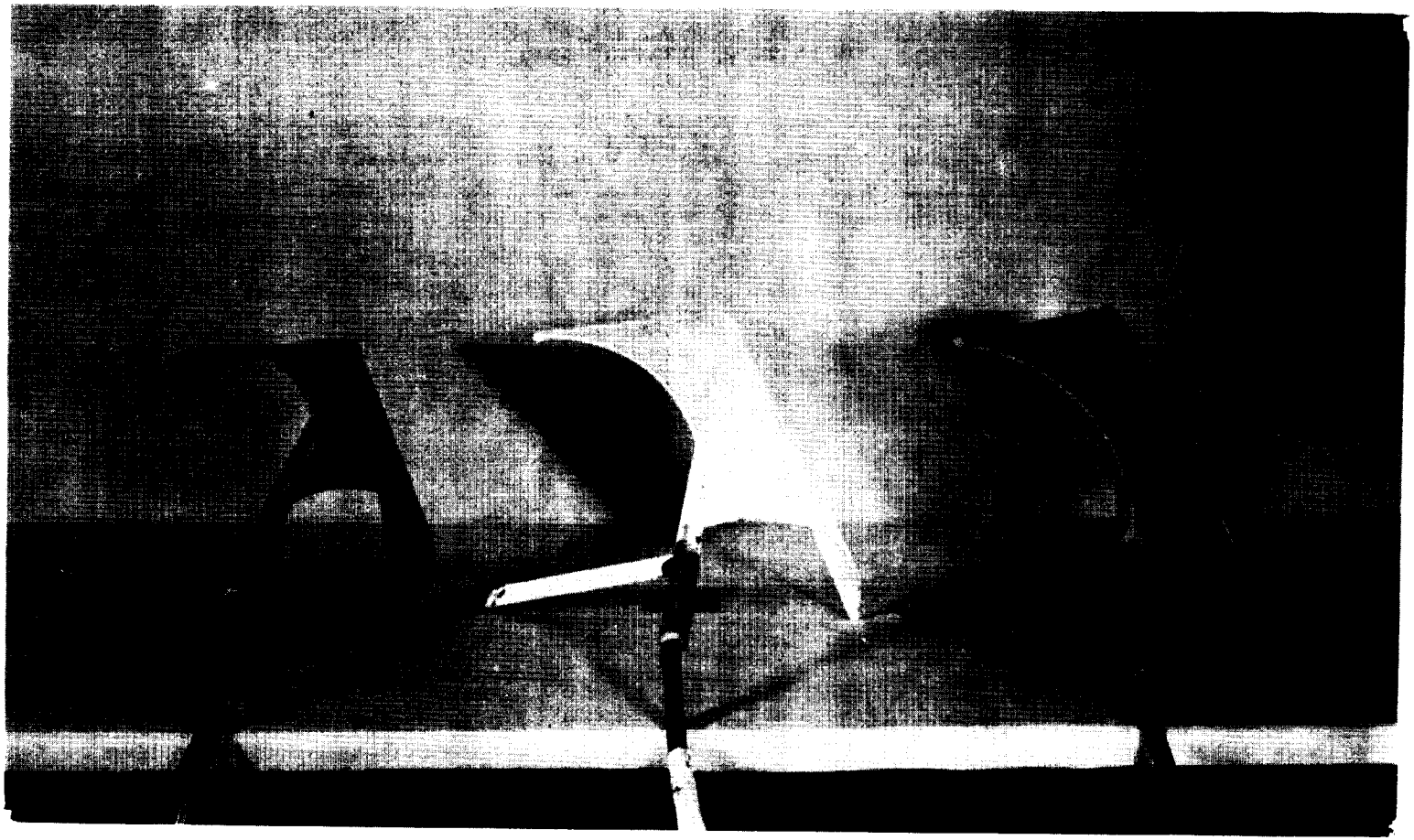

Model 1 Model 2 Model 3

(a) One-quarter rear view. L-61-4687

Figure 2.- Photograph of model.

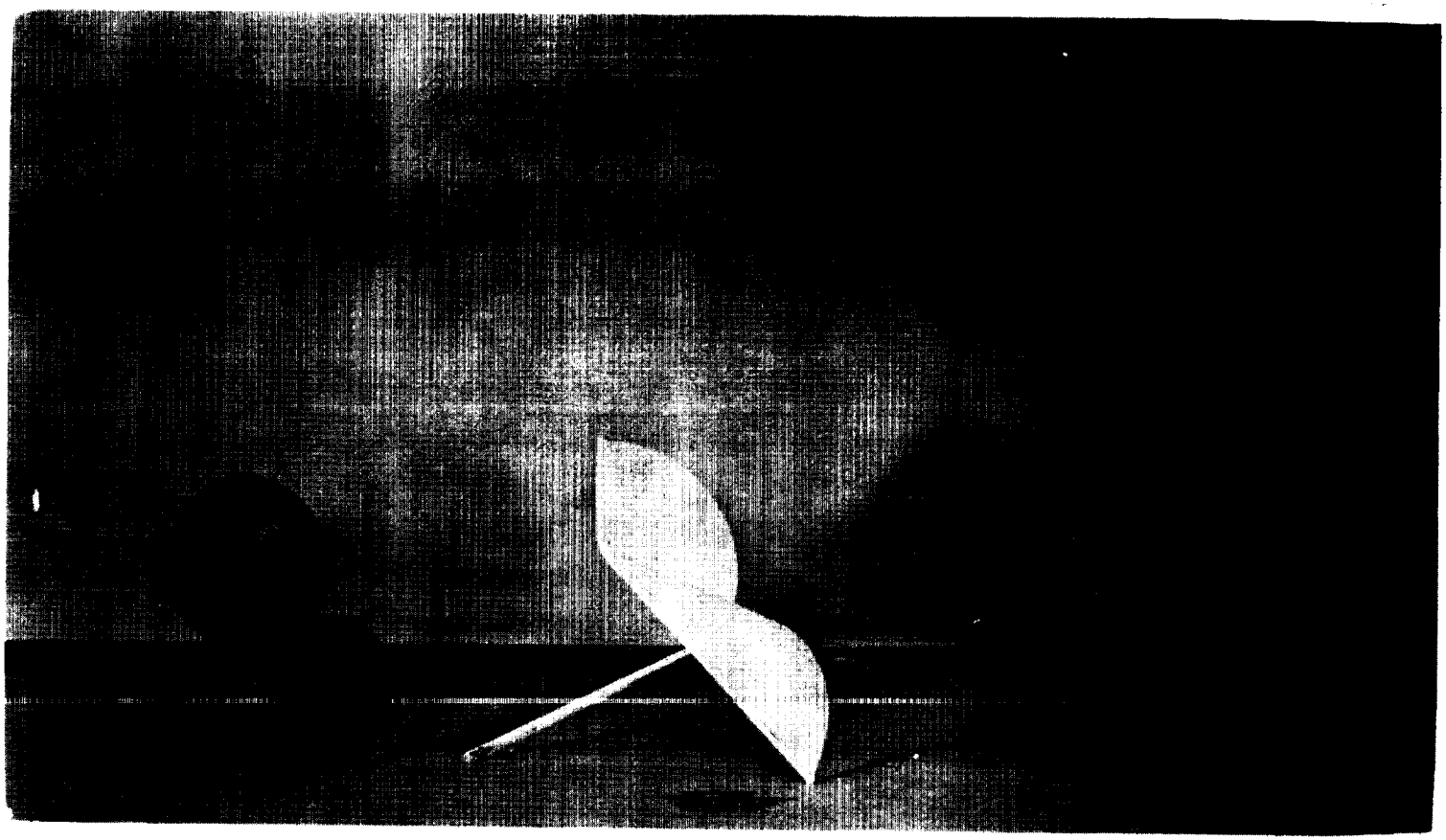

Model 1 Model 2 Model 3

(b) Three-quarter front view. L-61-4689

Figure 2.- Concluded.

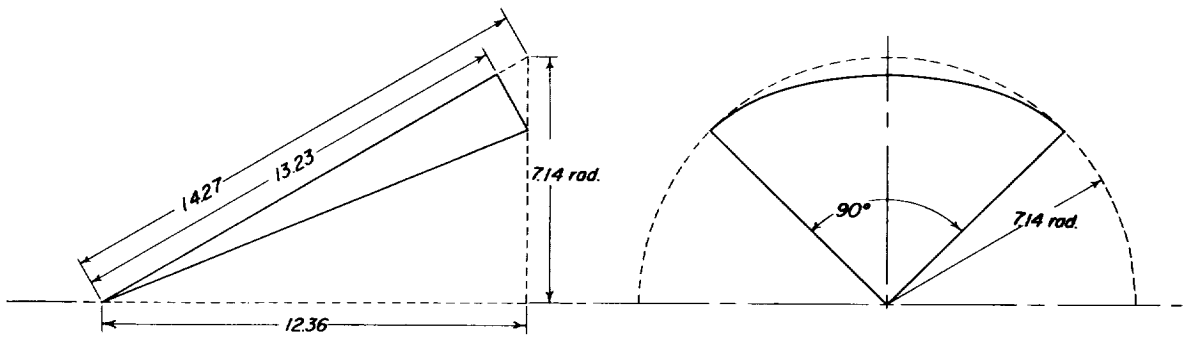

Model 3

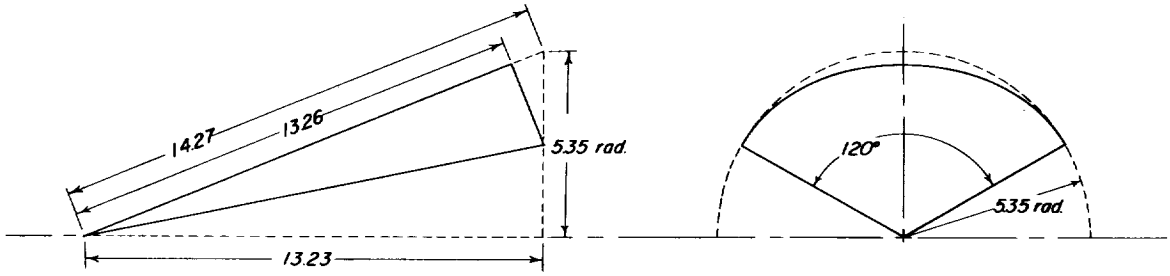

Model 2

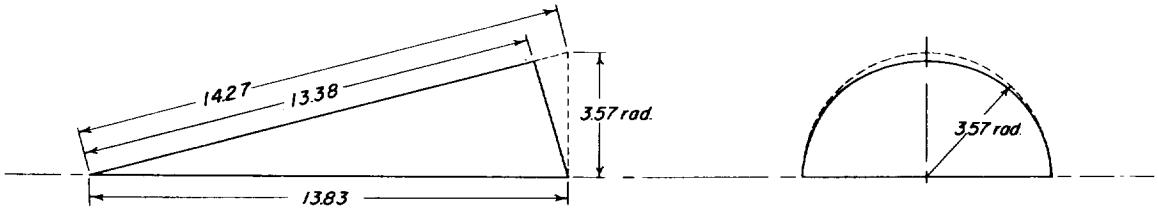

Model 1

Figure 3.- Development of paraglider panels. Dimensions are in inches.

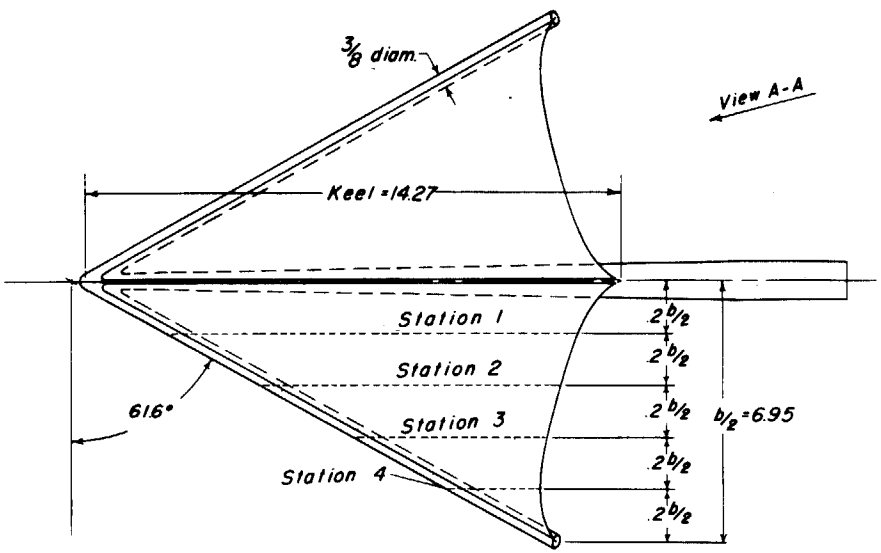

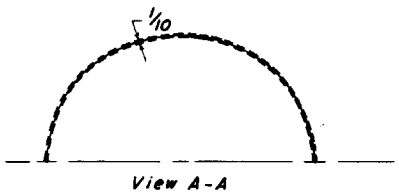

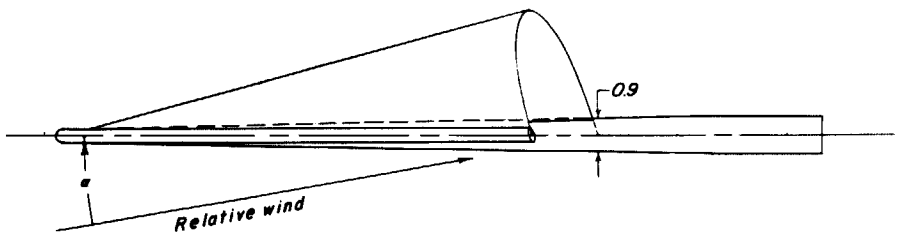

(a) Model 1.

Figure 4.- Geometric characteristics of rigid paraglider models. Dimensions are in inches.

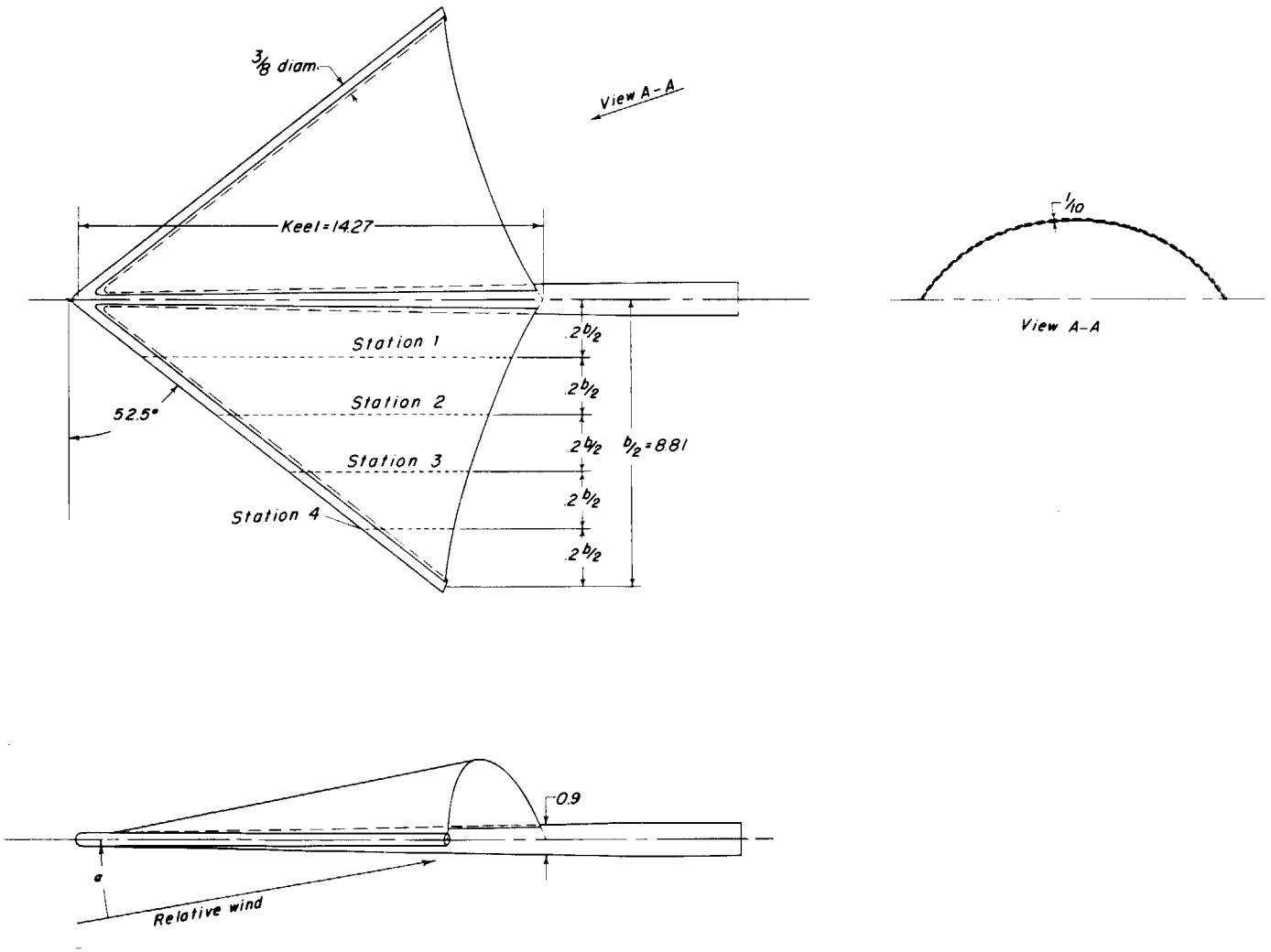

(b) Model 2.

Figure 4.- Continued.

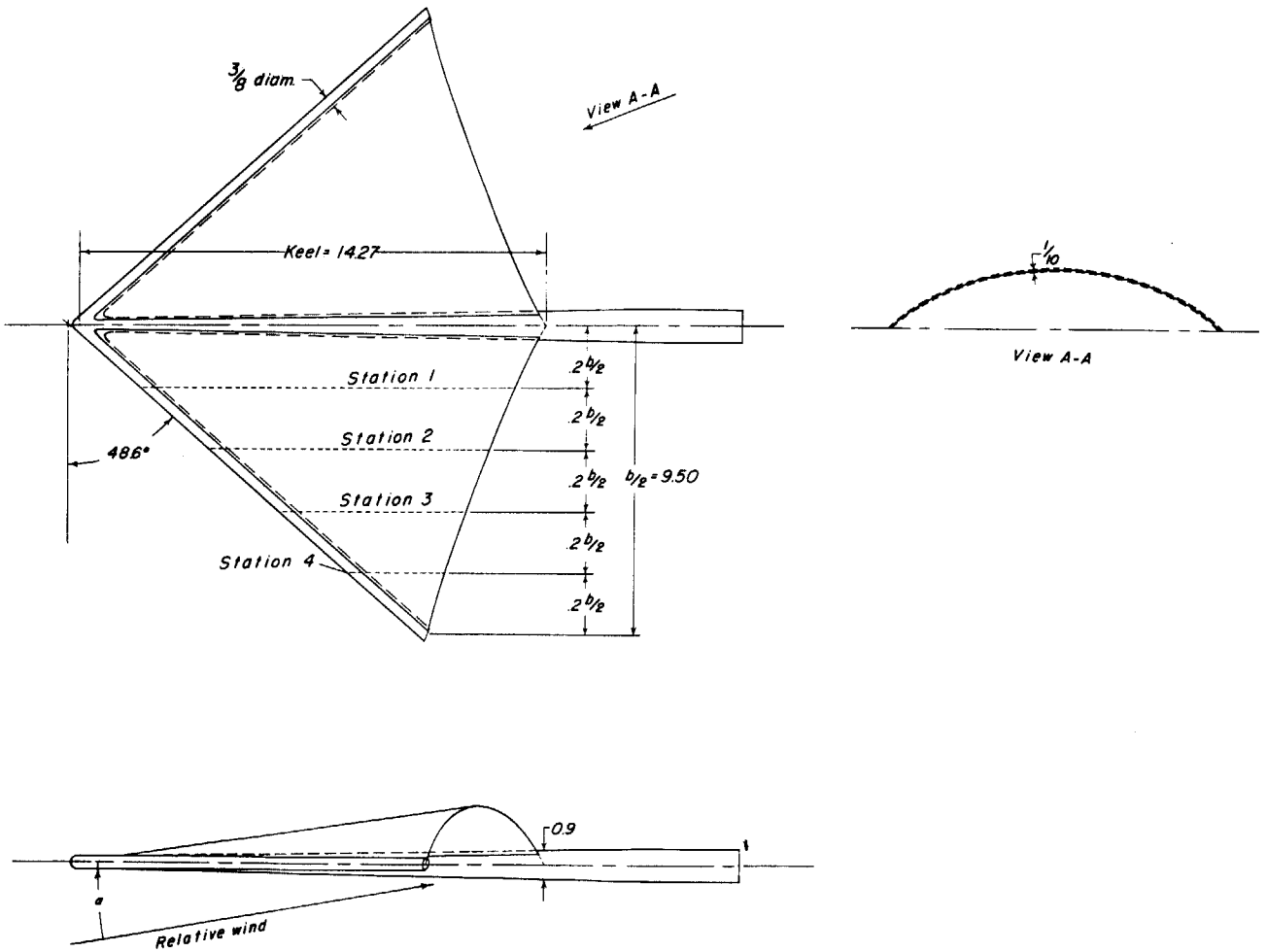

(c) Model 3.

Figure 4.- Concluded.

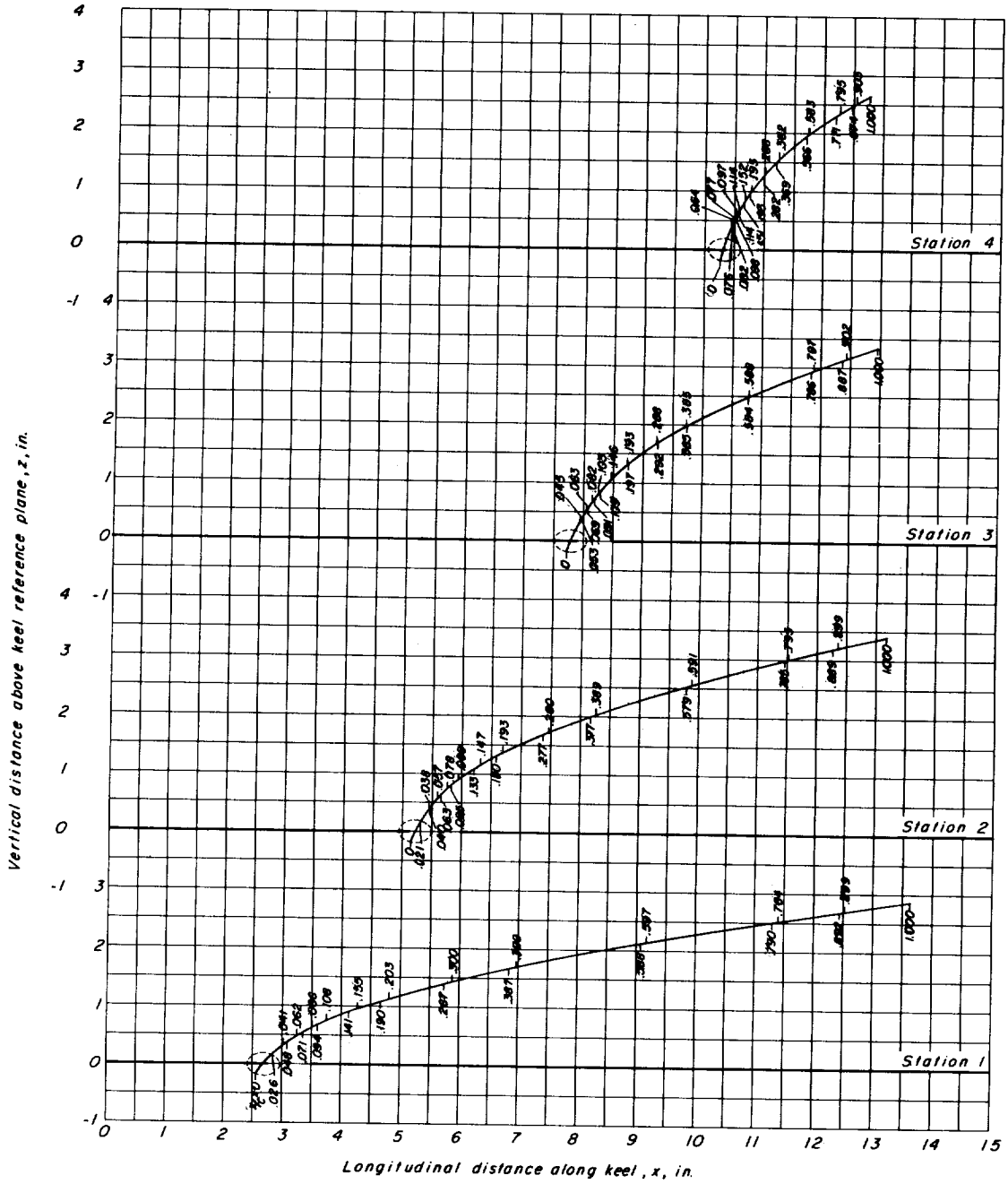

(a) Model 1.

Figure 5.- Location of lower- and upper-surface orifices designated in fraction of local projected chord.

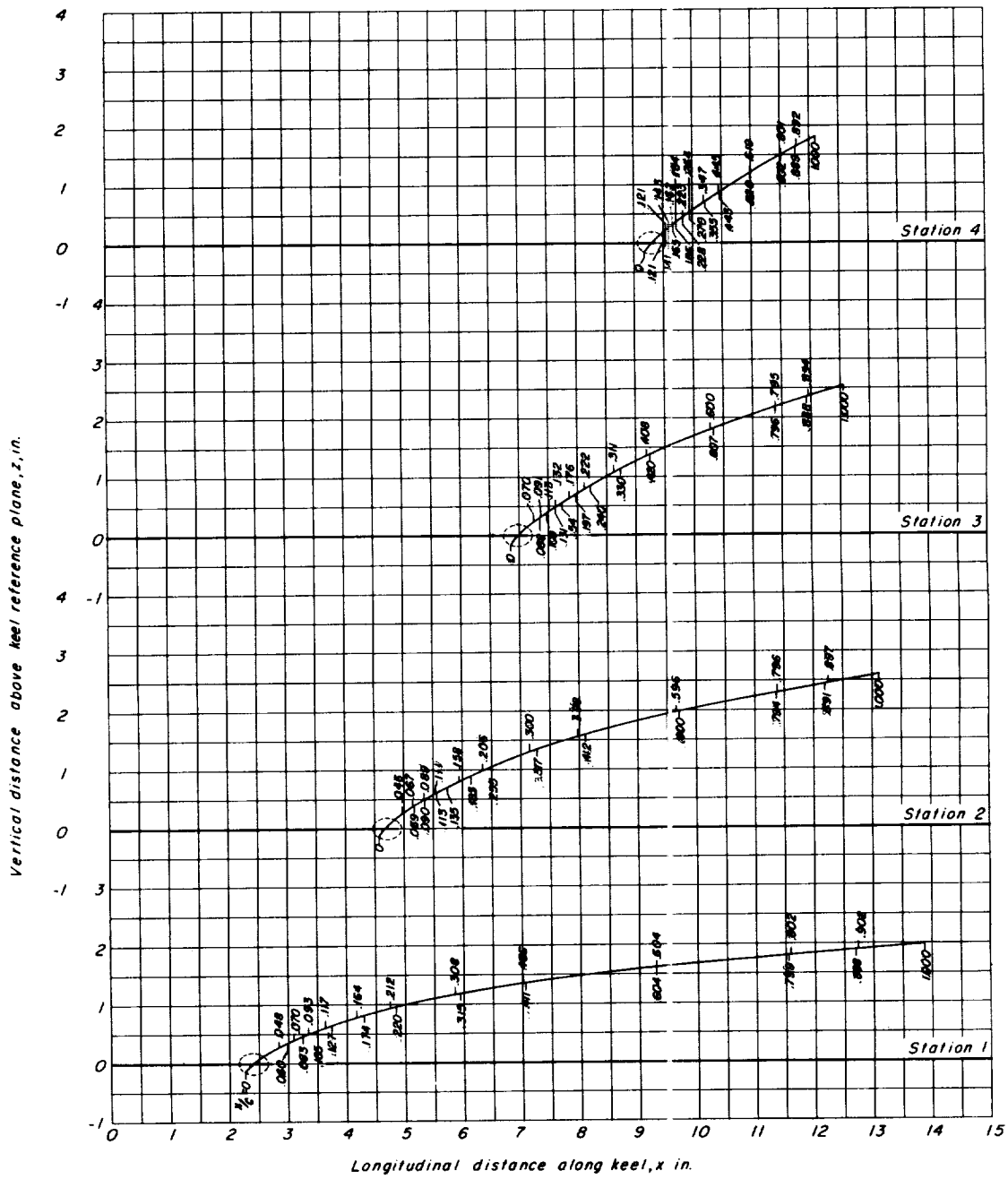

(b) Model 2.

Figure 5.- Continued.

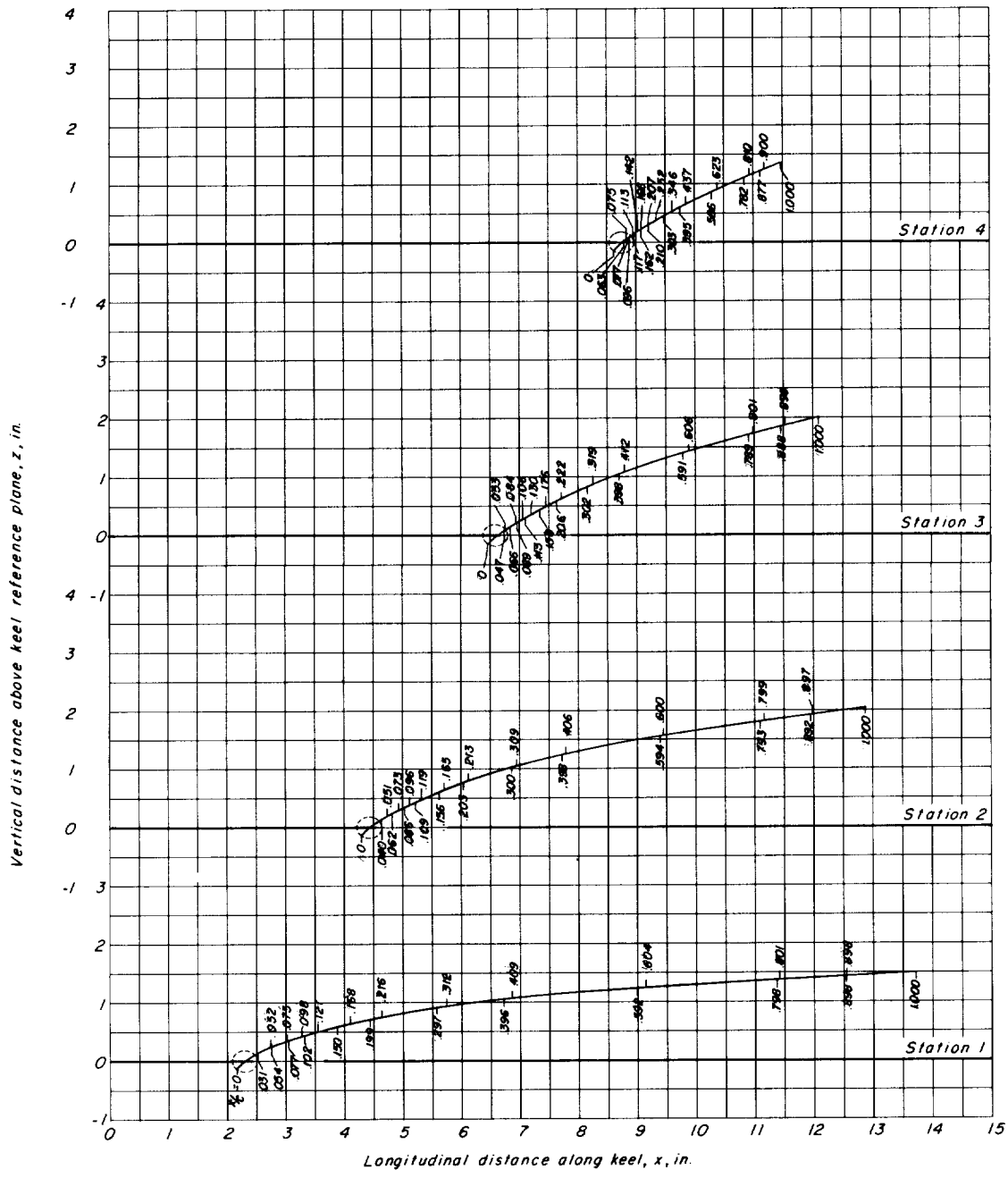

(c) Model 3.

Figure 5.- Concluded.

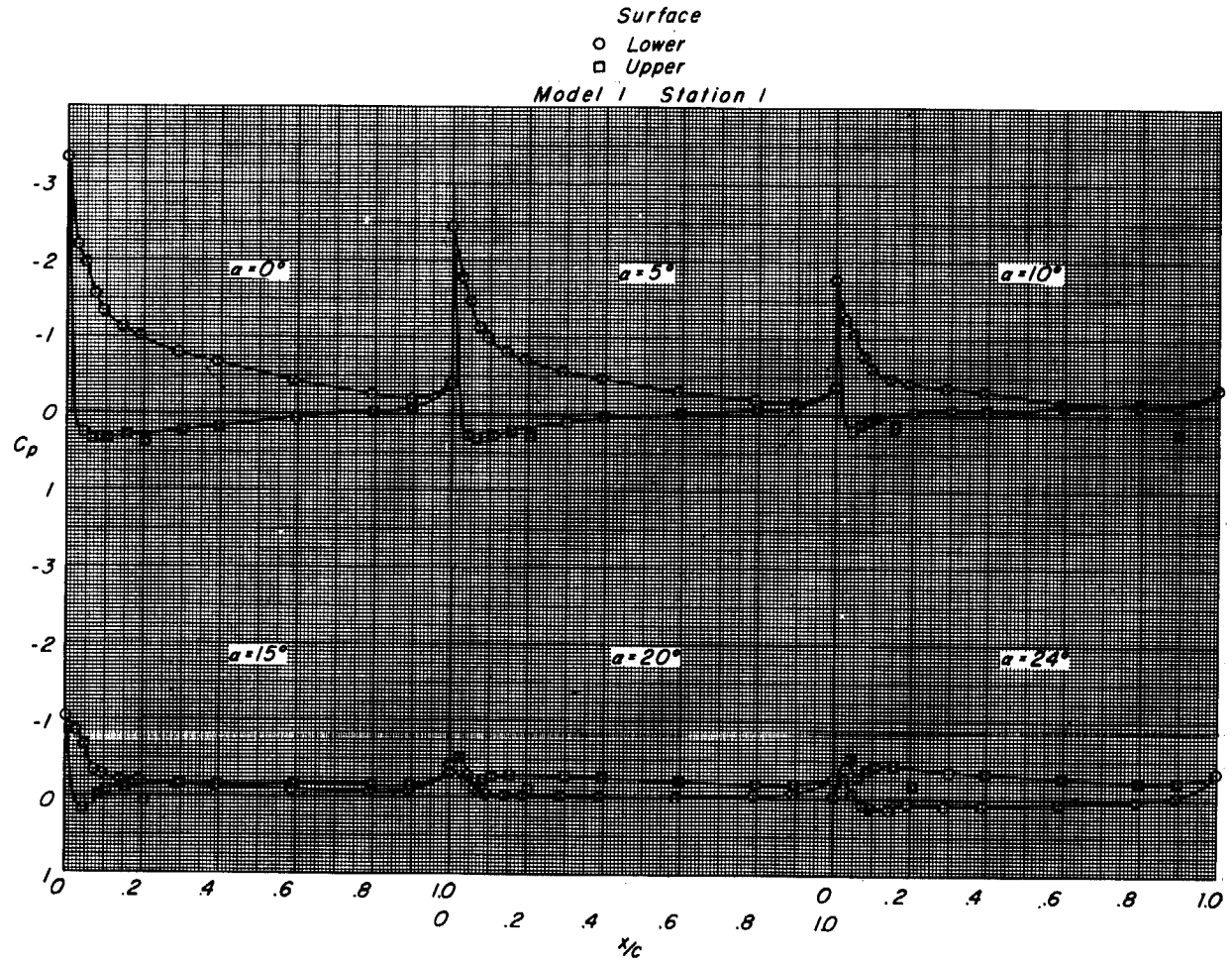

(a) Station 1.

Figure 6.- Pressure distributions on model 1 at various angles of attack.

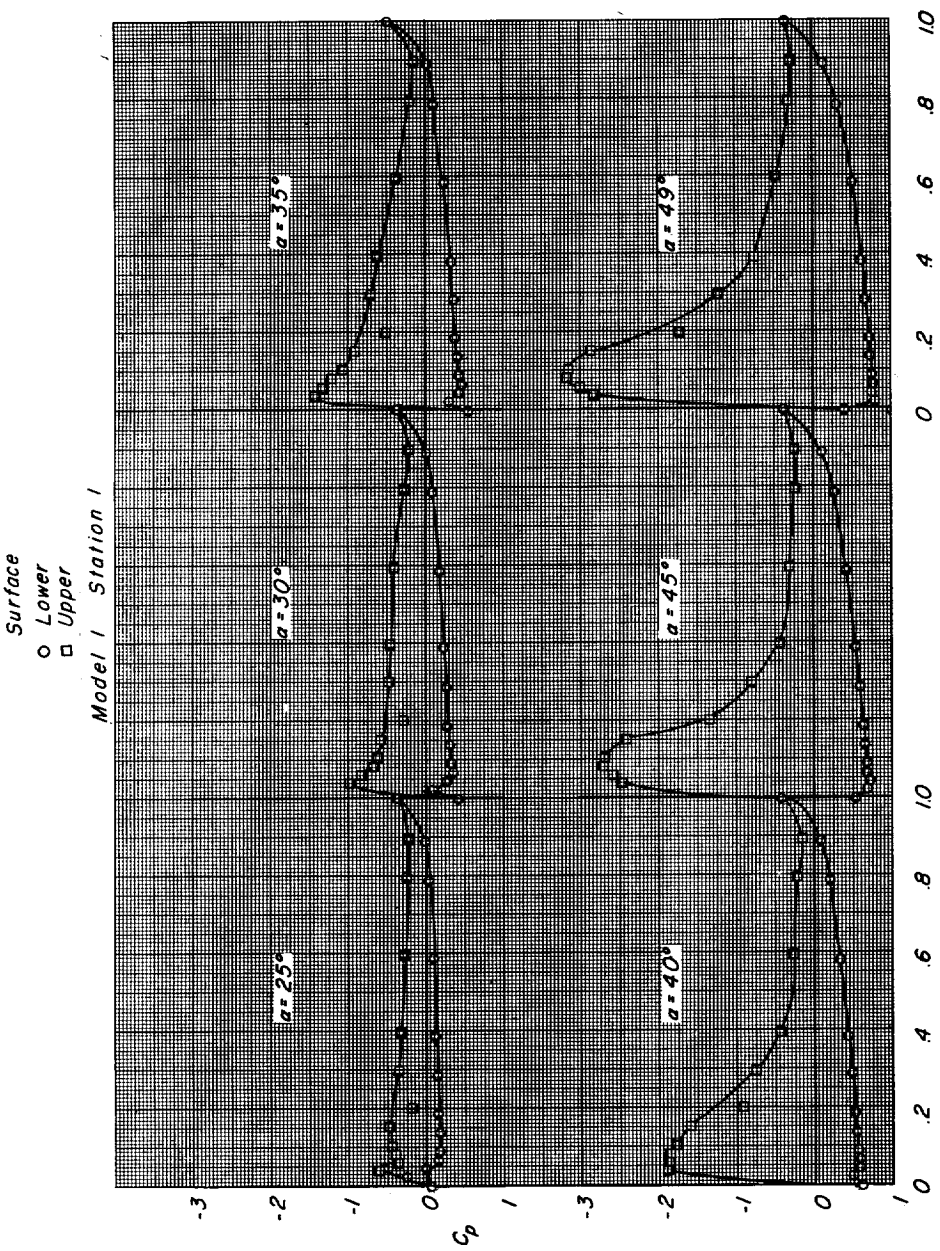

(a) Continued.

Figure 6.- Continued.

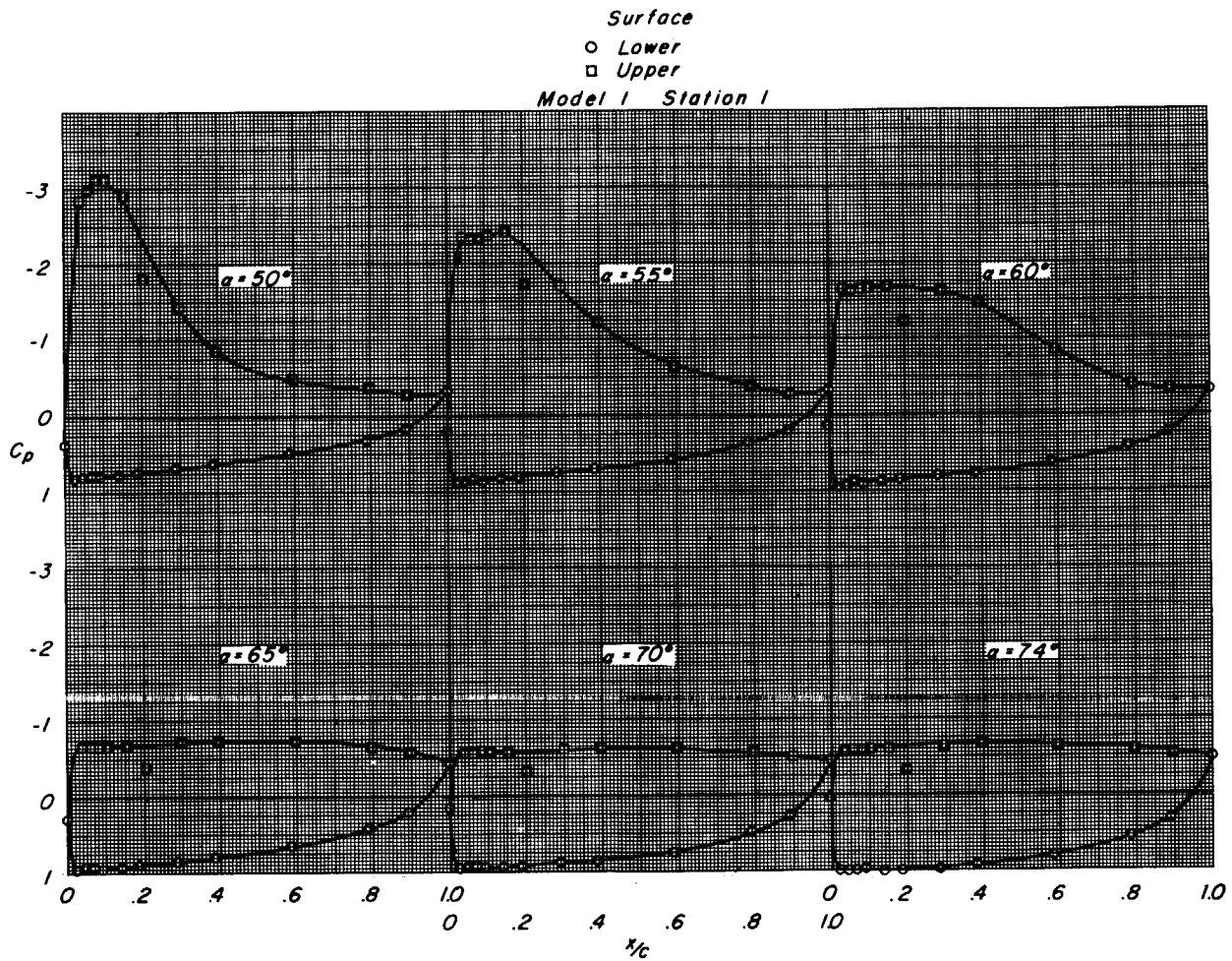

(a) Concluded.

Figure 6.- Continued.

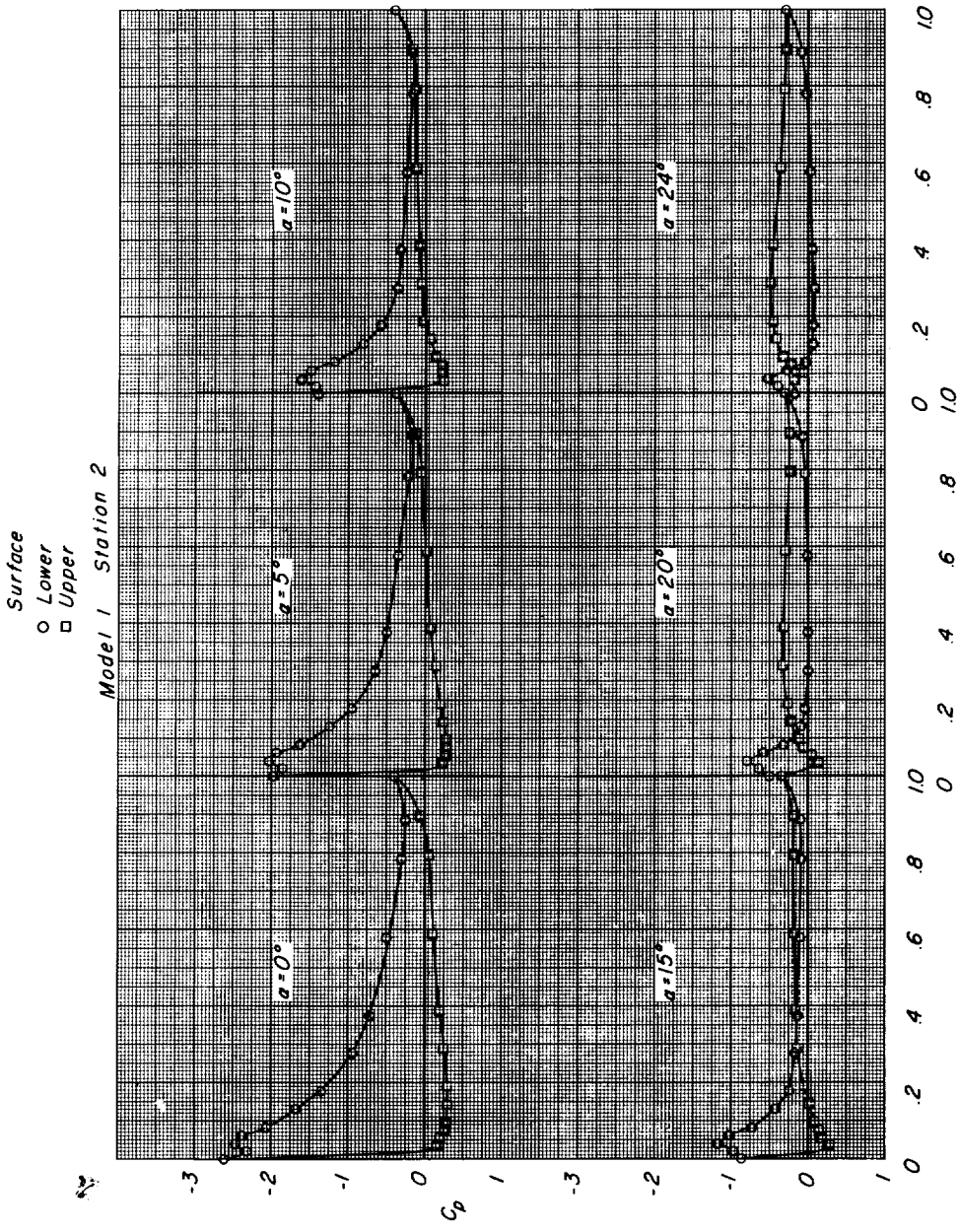

(b) Station 2.

Figure 6.- Continued.

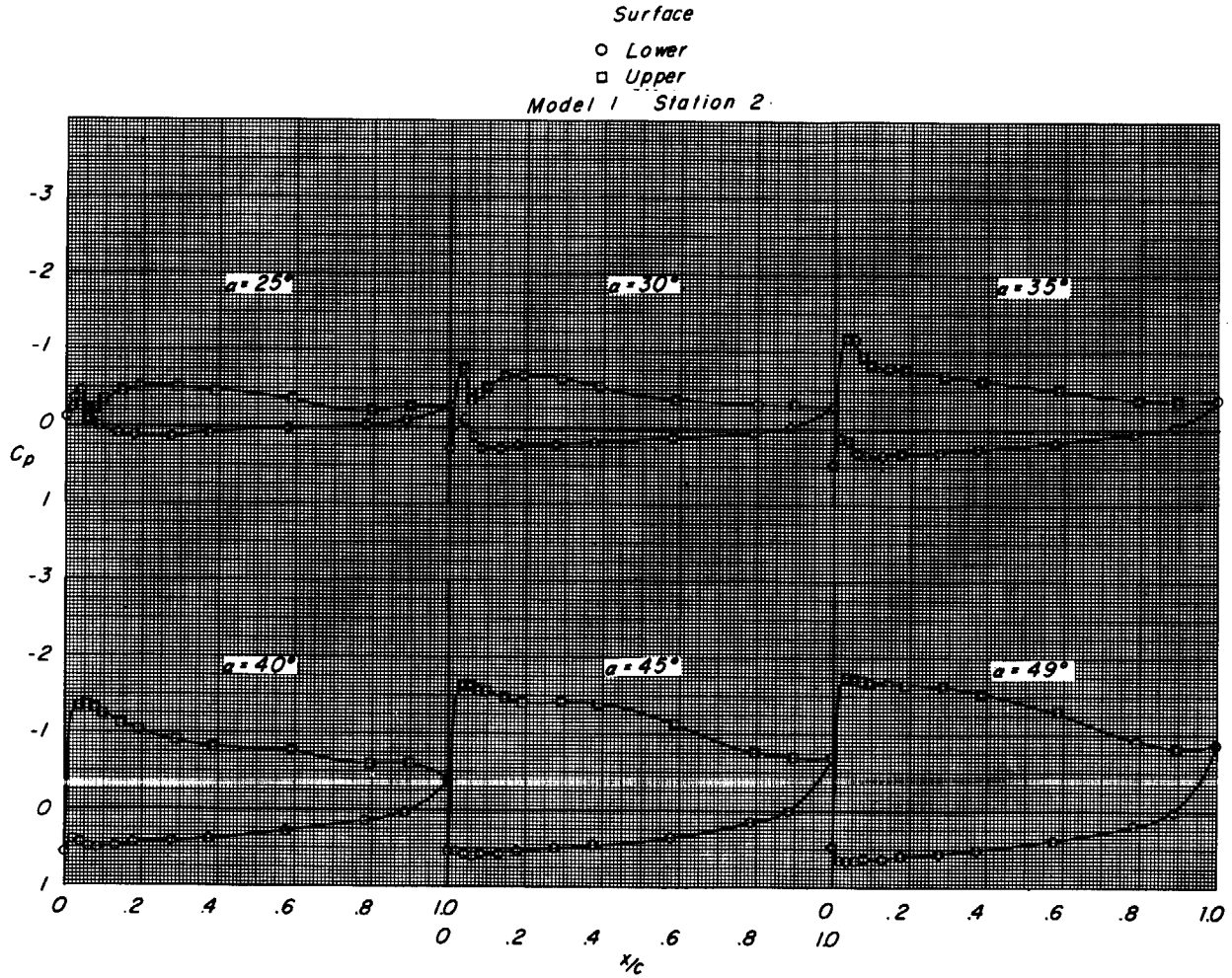

(b) Continued.

Figure 6.- Continued.

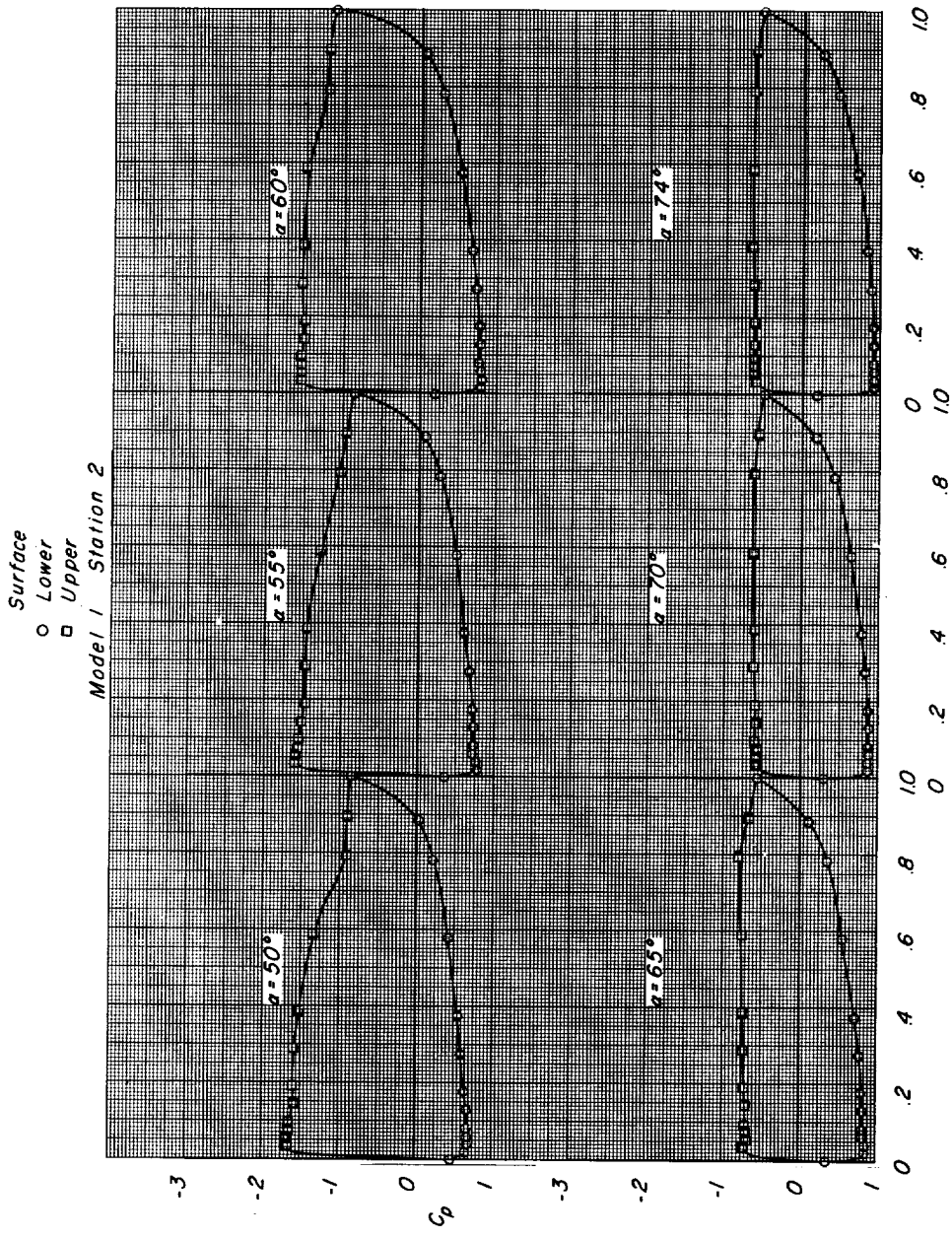

(b) Concluded.

Figure 6.- Continued.

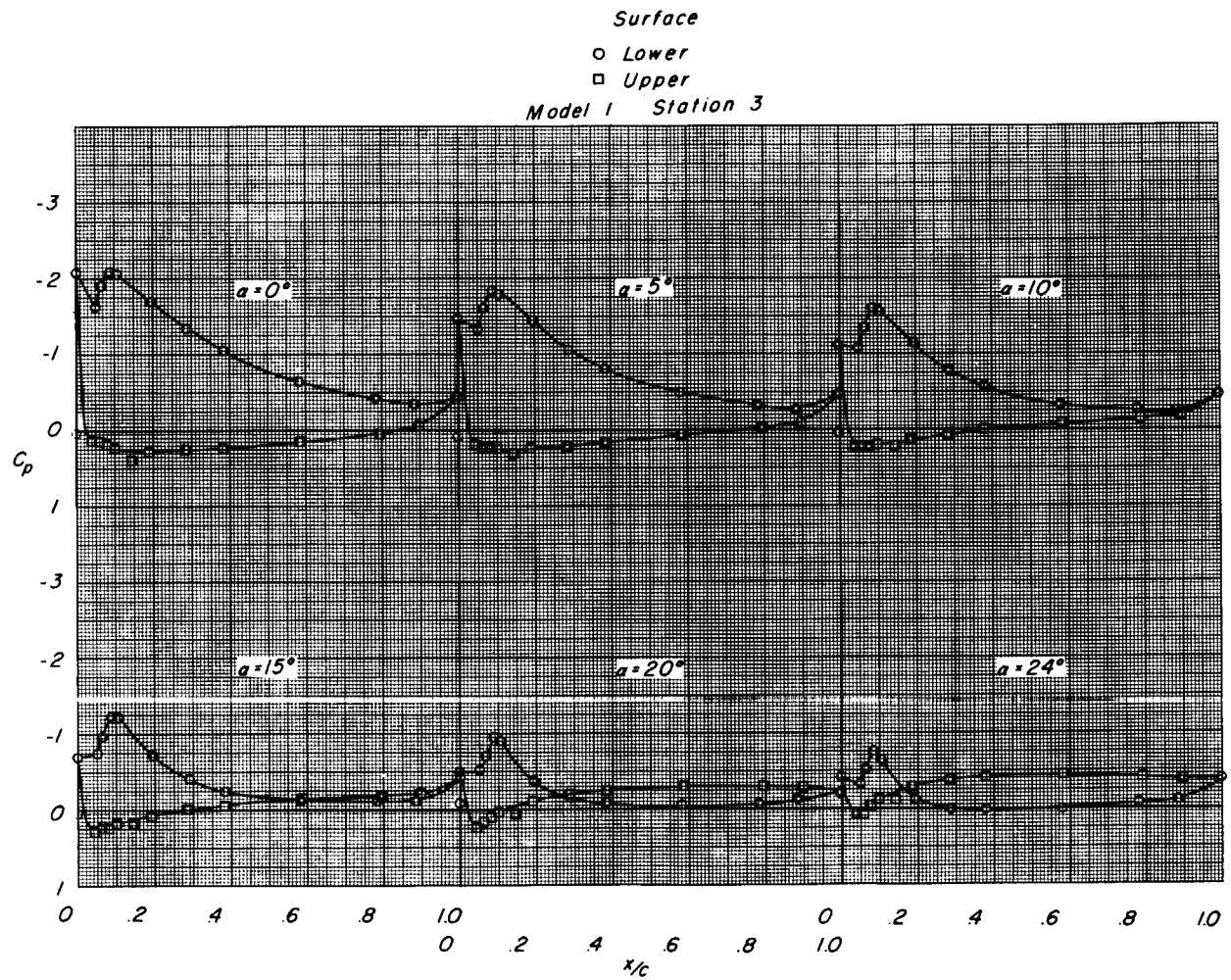

(c) Station 3.

Figure 6.- Continued.

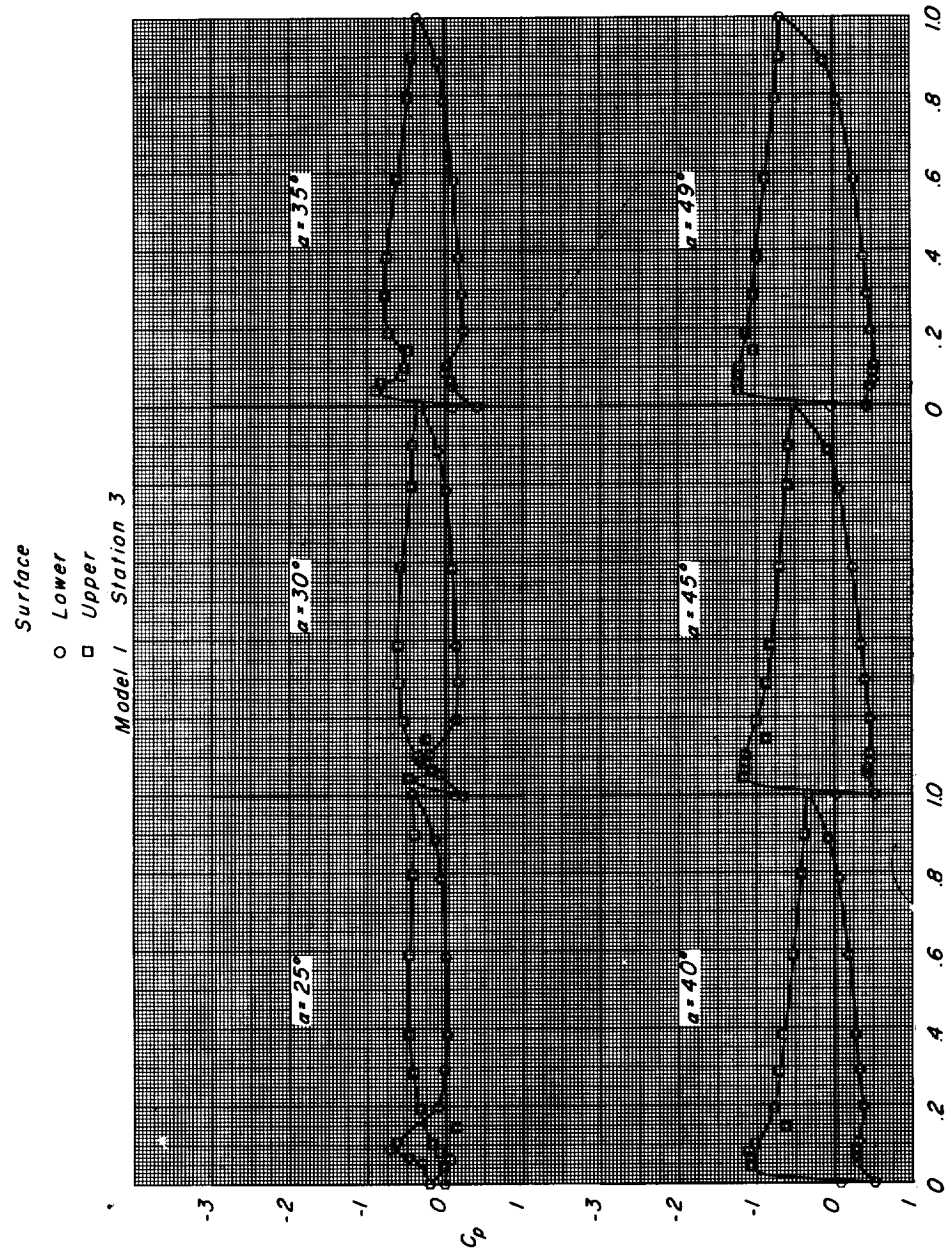

(c) Continued.

Figure 6.- Continued.

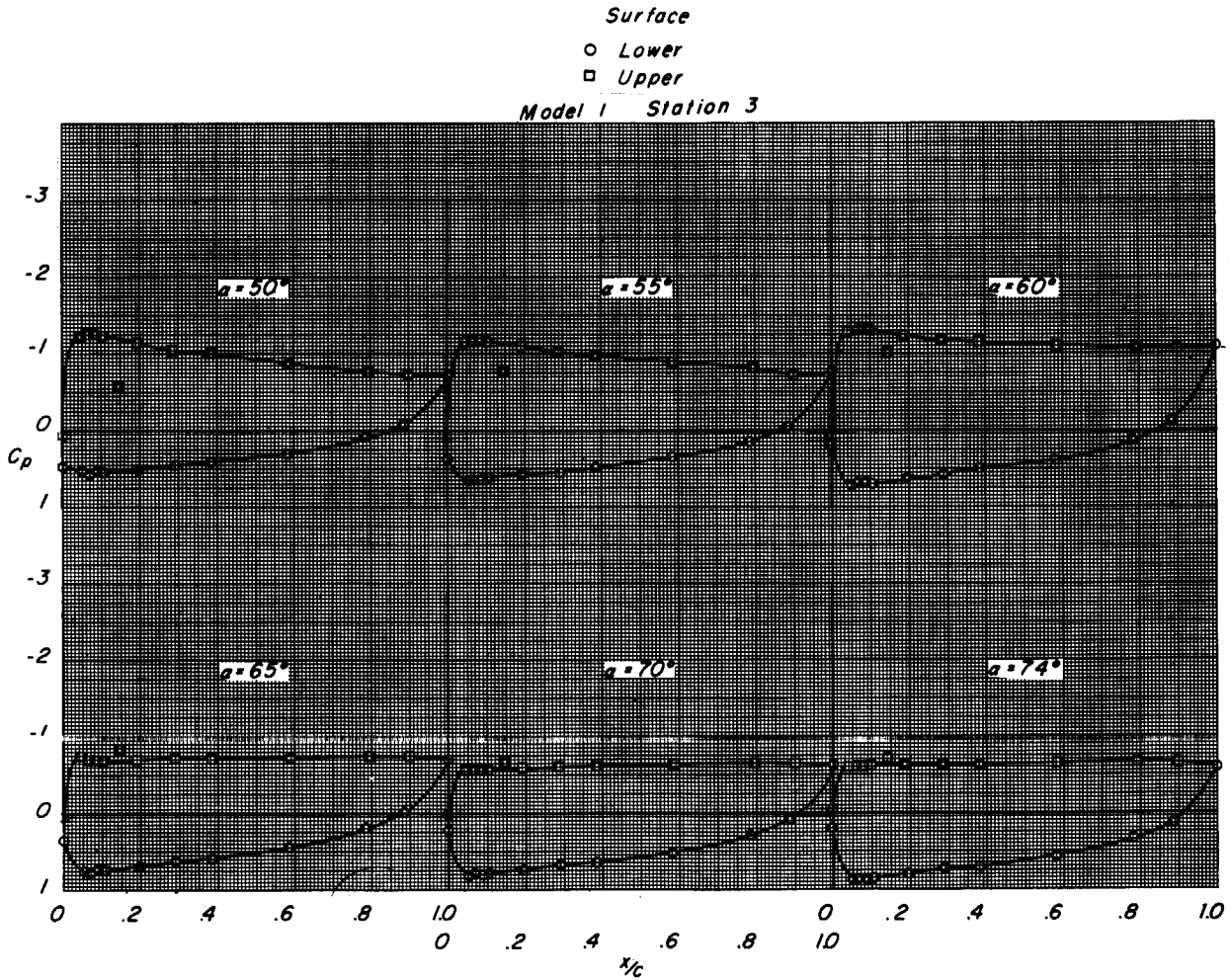

(c) Concluded.

Figure 6.- Continued.

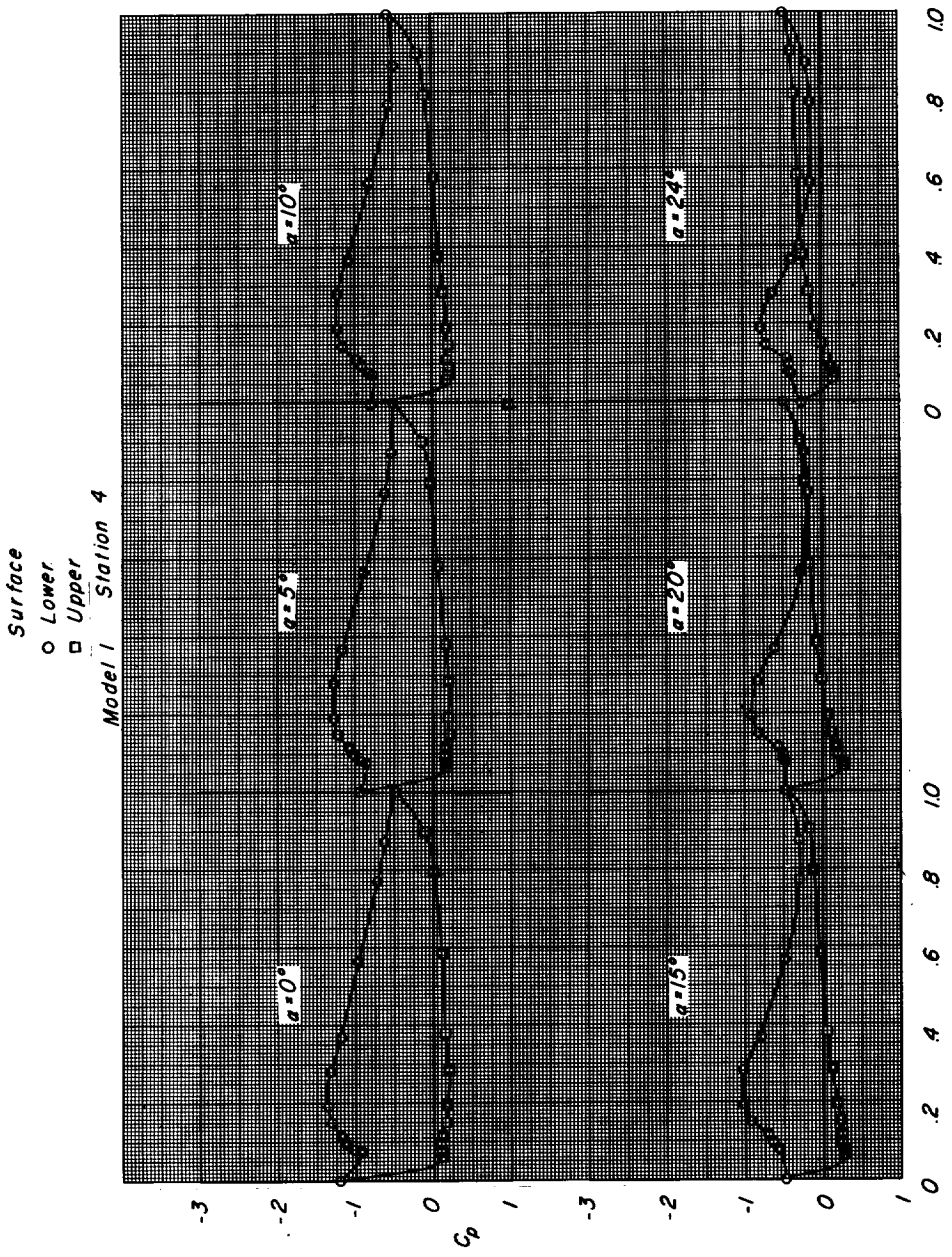

(d) Station 4.

Figure 6.- Continued.

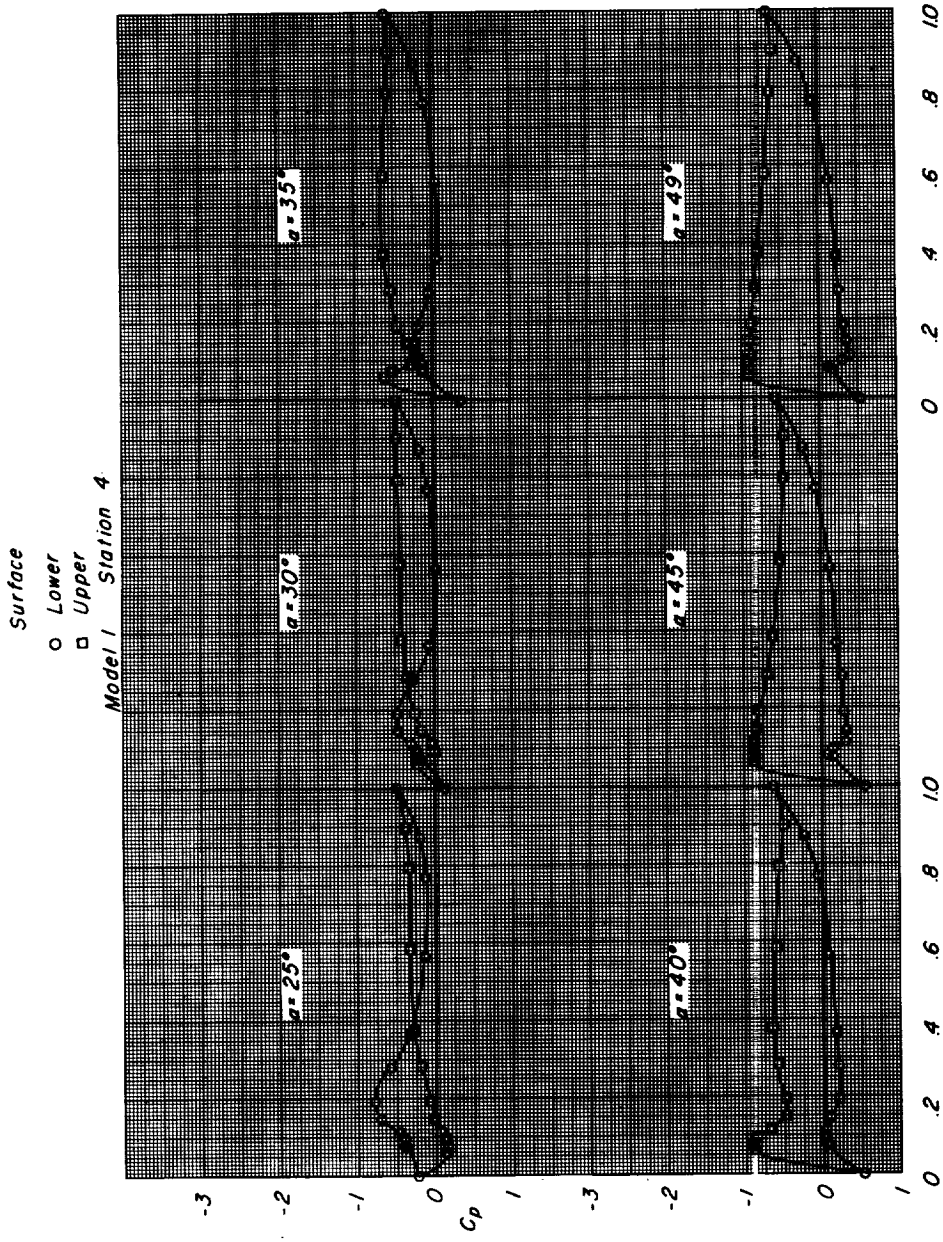

(d) Continued.

Figure 6.- Continued.

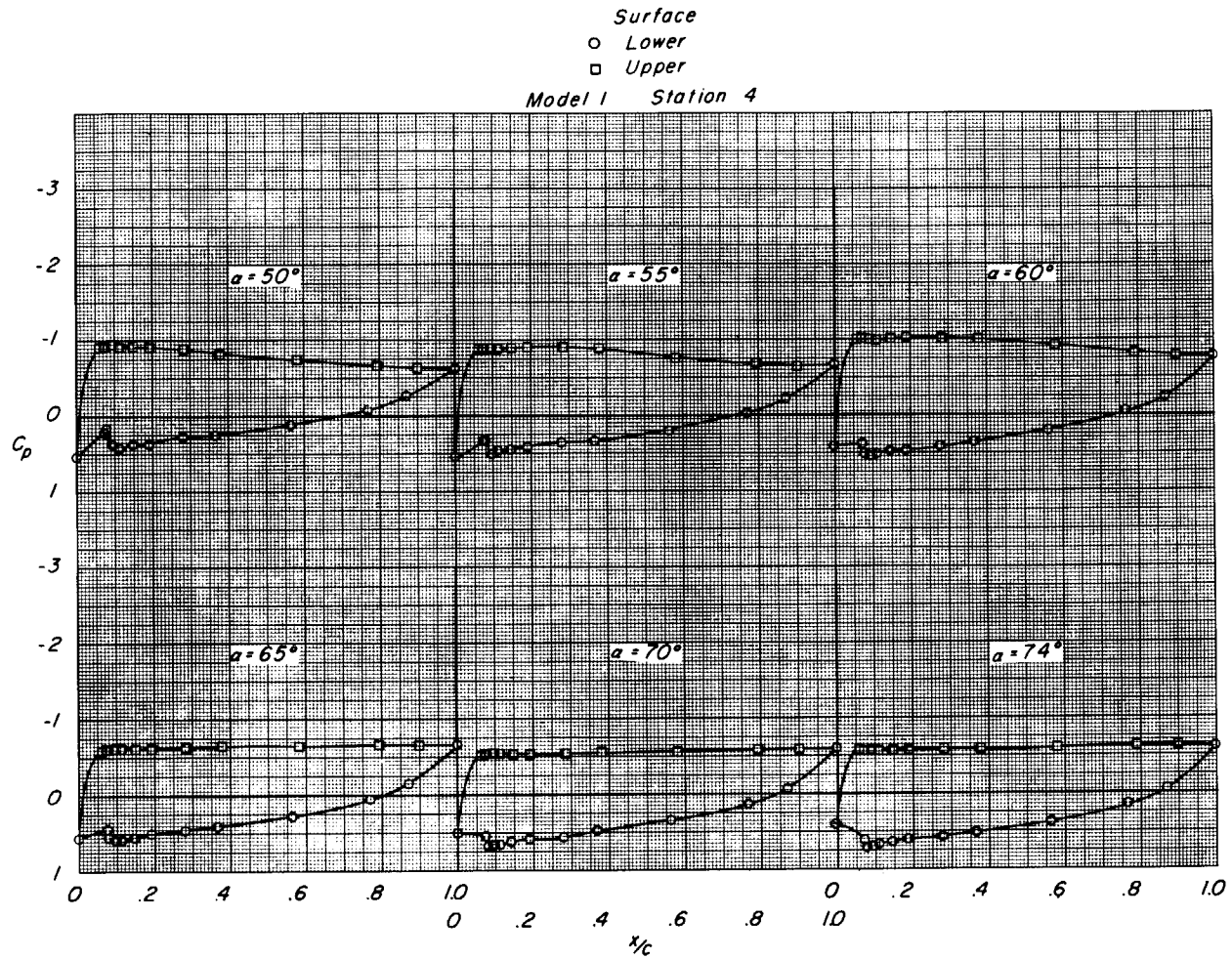

(d) Concluded.

Figure 6.- Concluded.

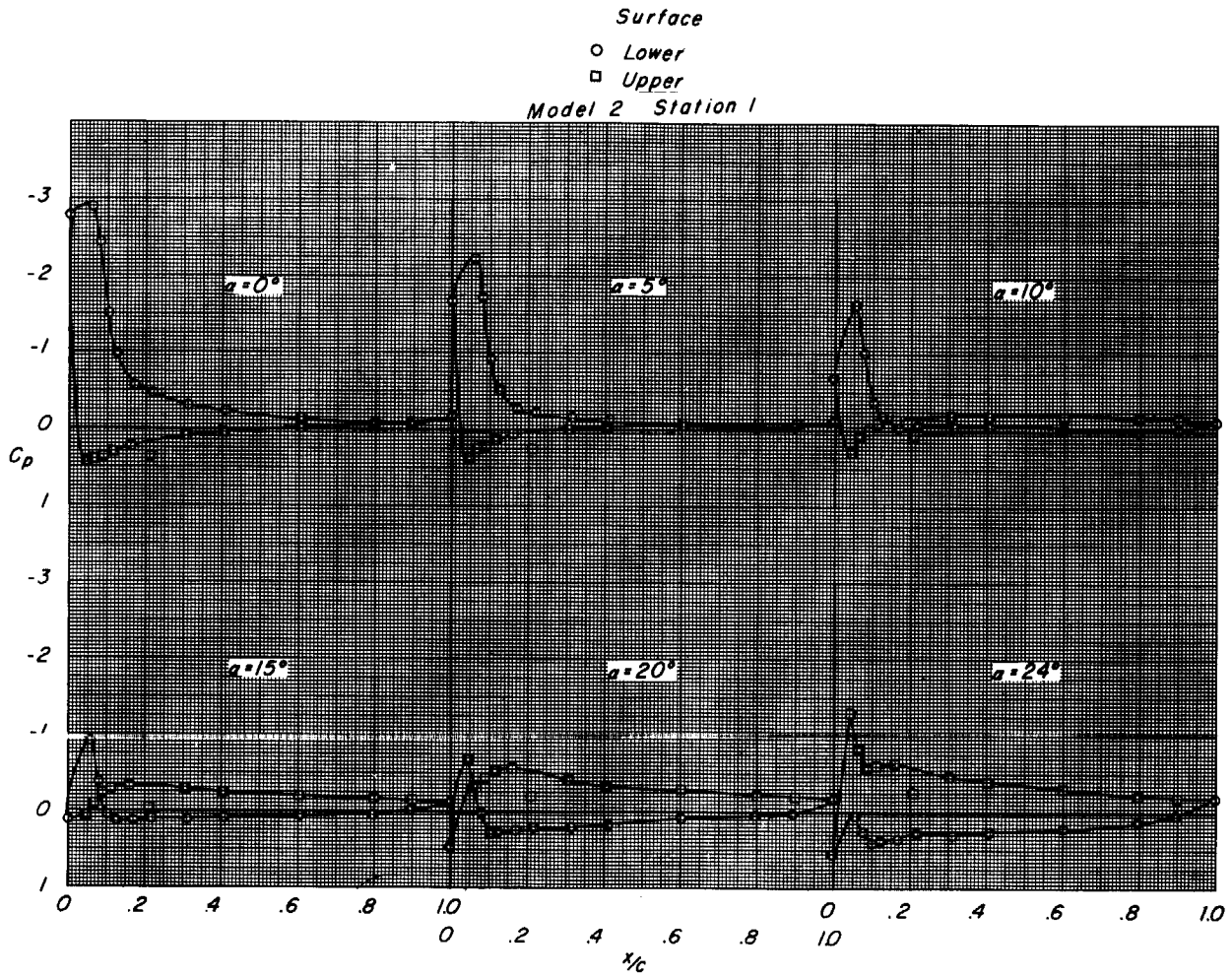

(a) Station 1.

Figure 7.- Pressure distributions on model 2 at various angles of attack.

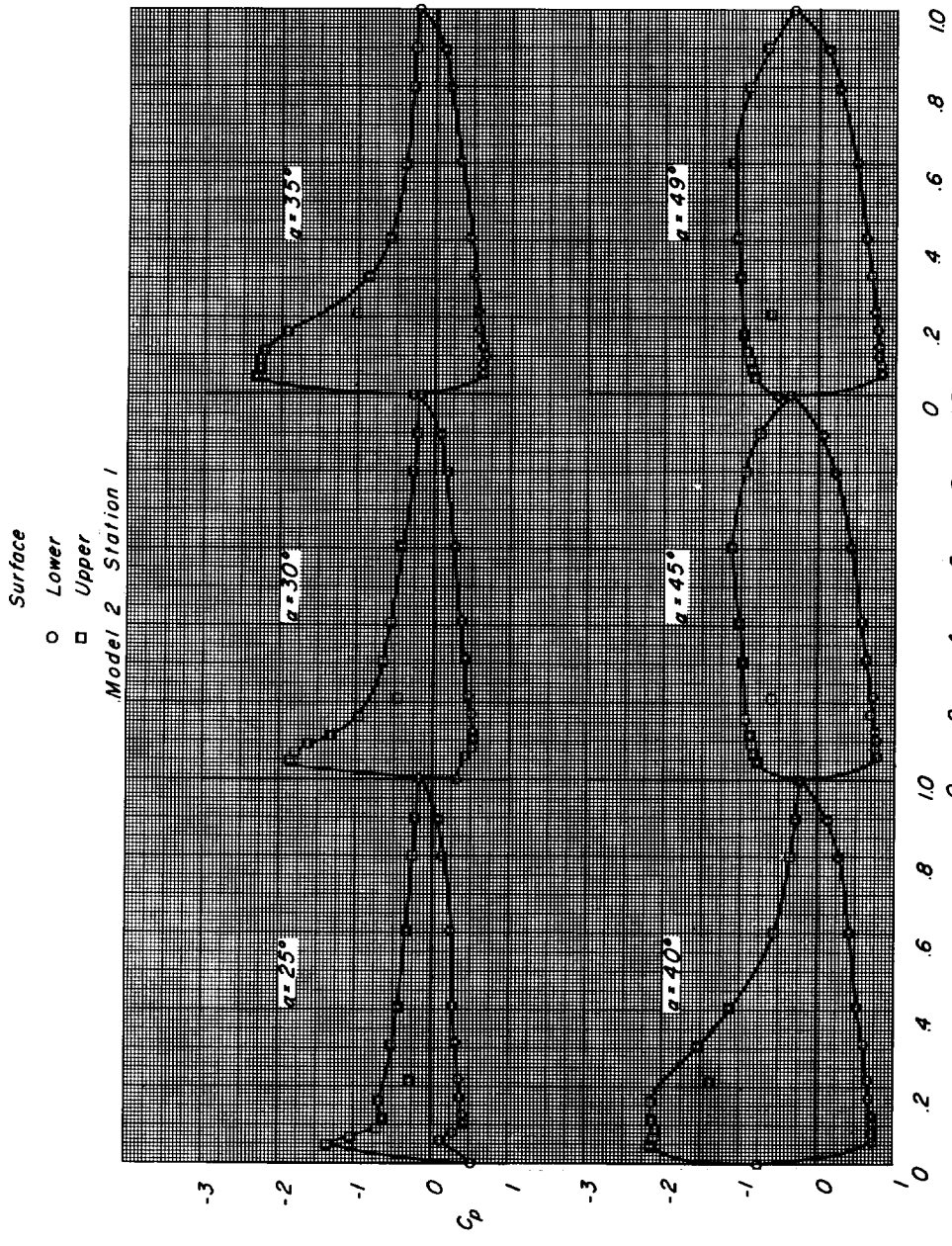

(a) Continued.

Figure 7.- Continued.

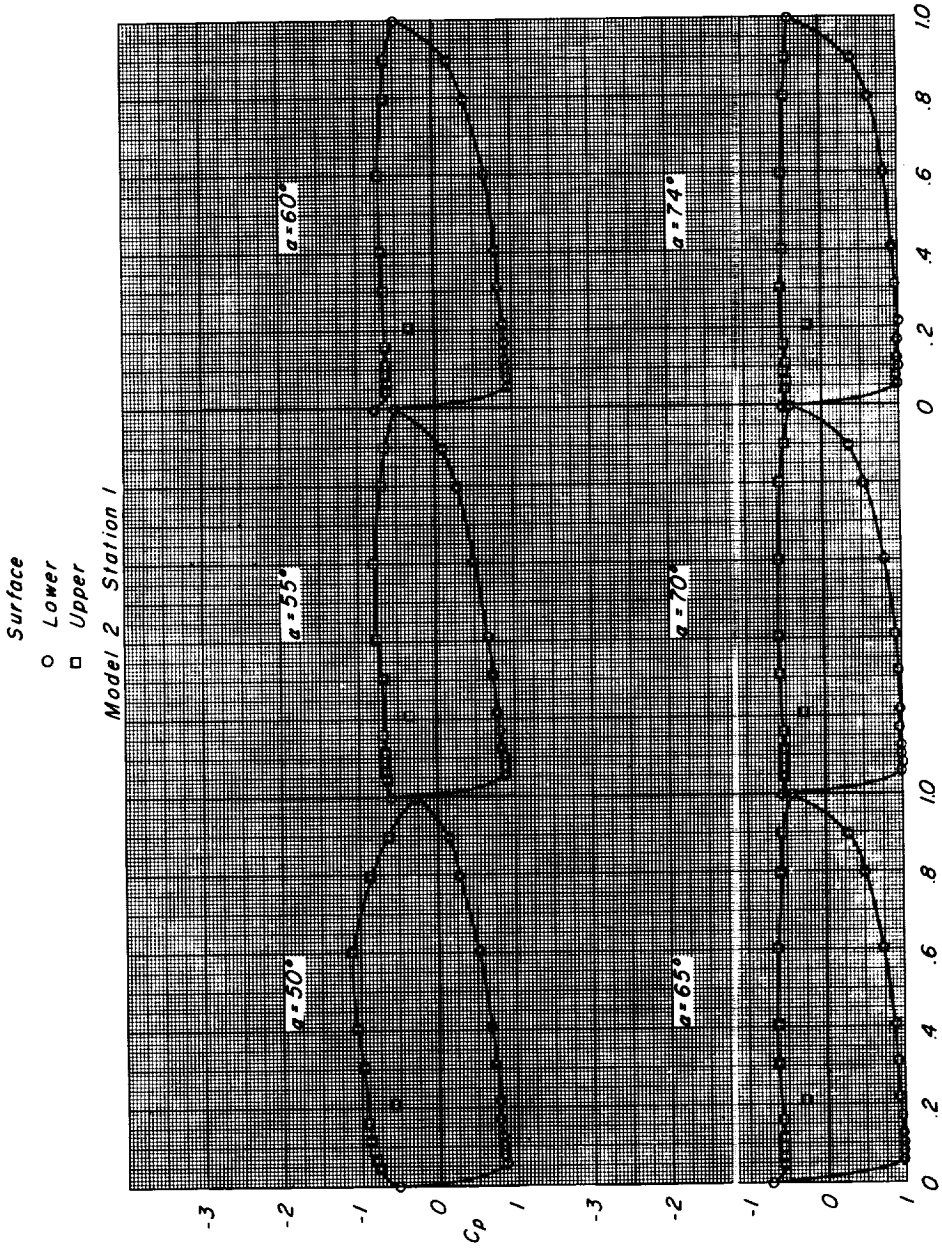

(a) Concluded.

Figure 7.- Continued.

L-1757

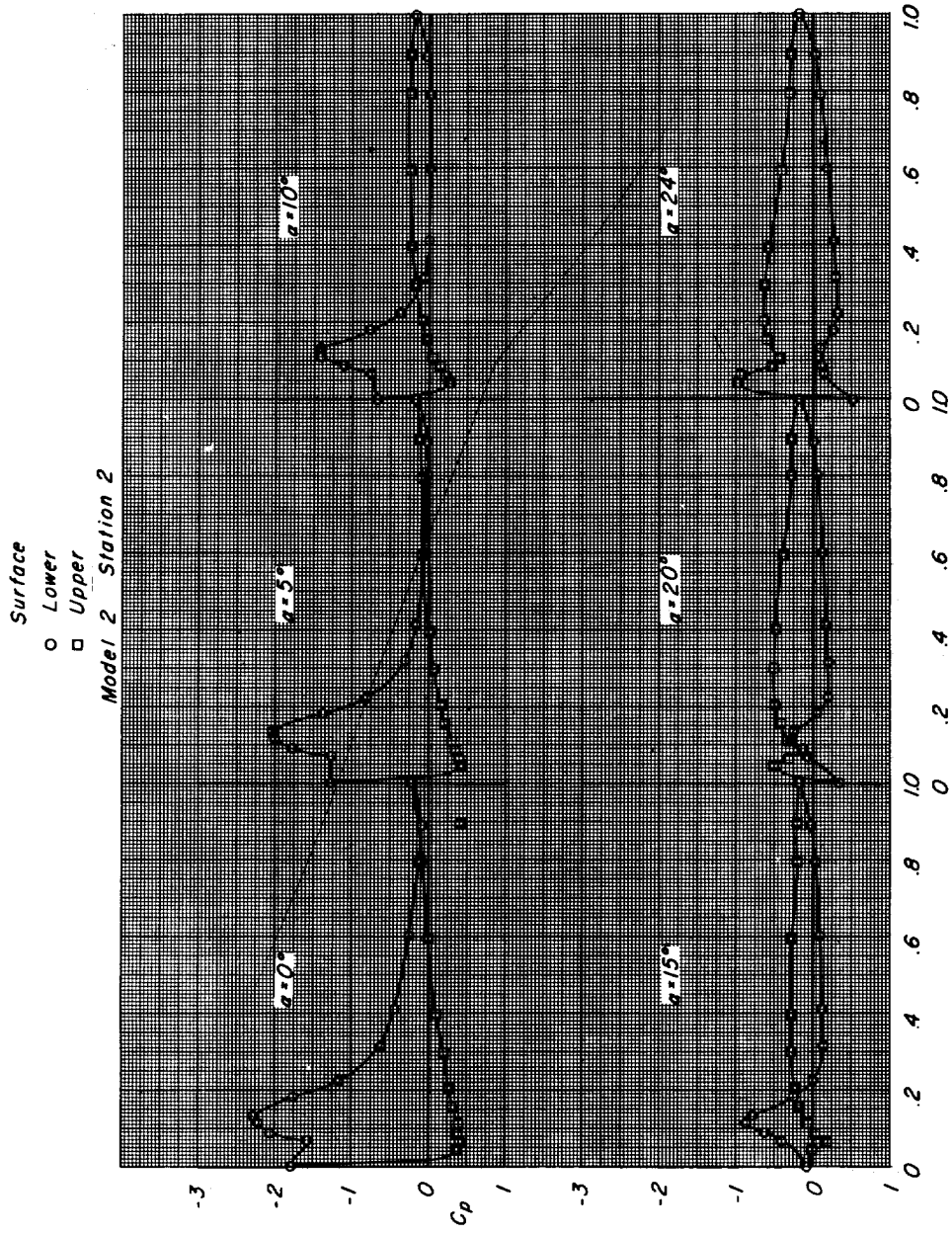

(b) Station 2.

Figure 7.- Continued.

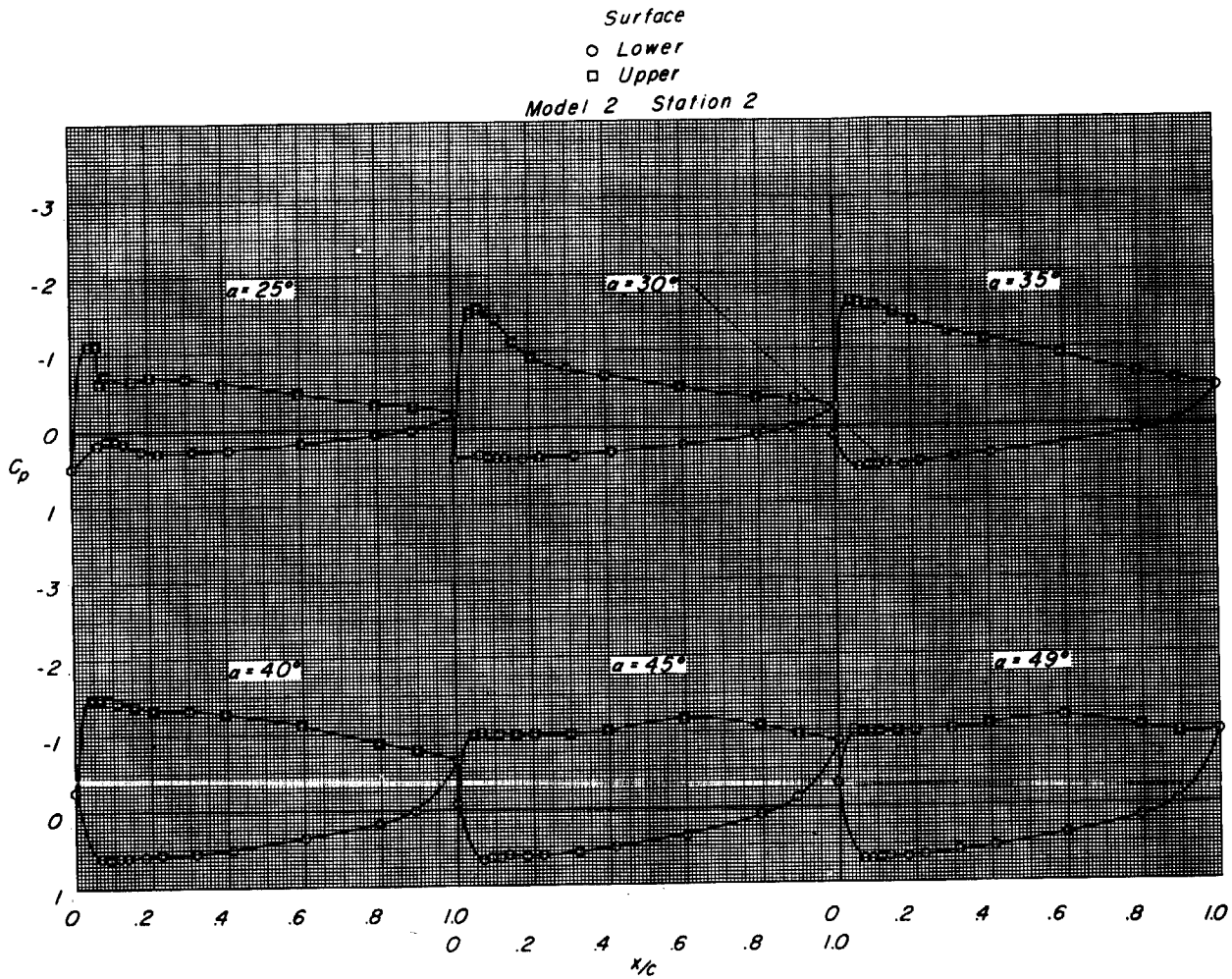

(b) Continued.

Figure 7.- Continued.

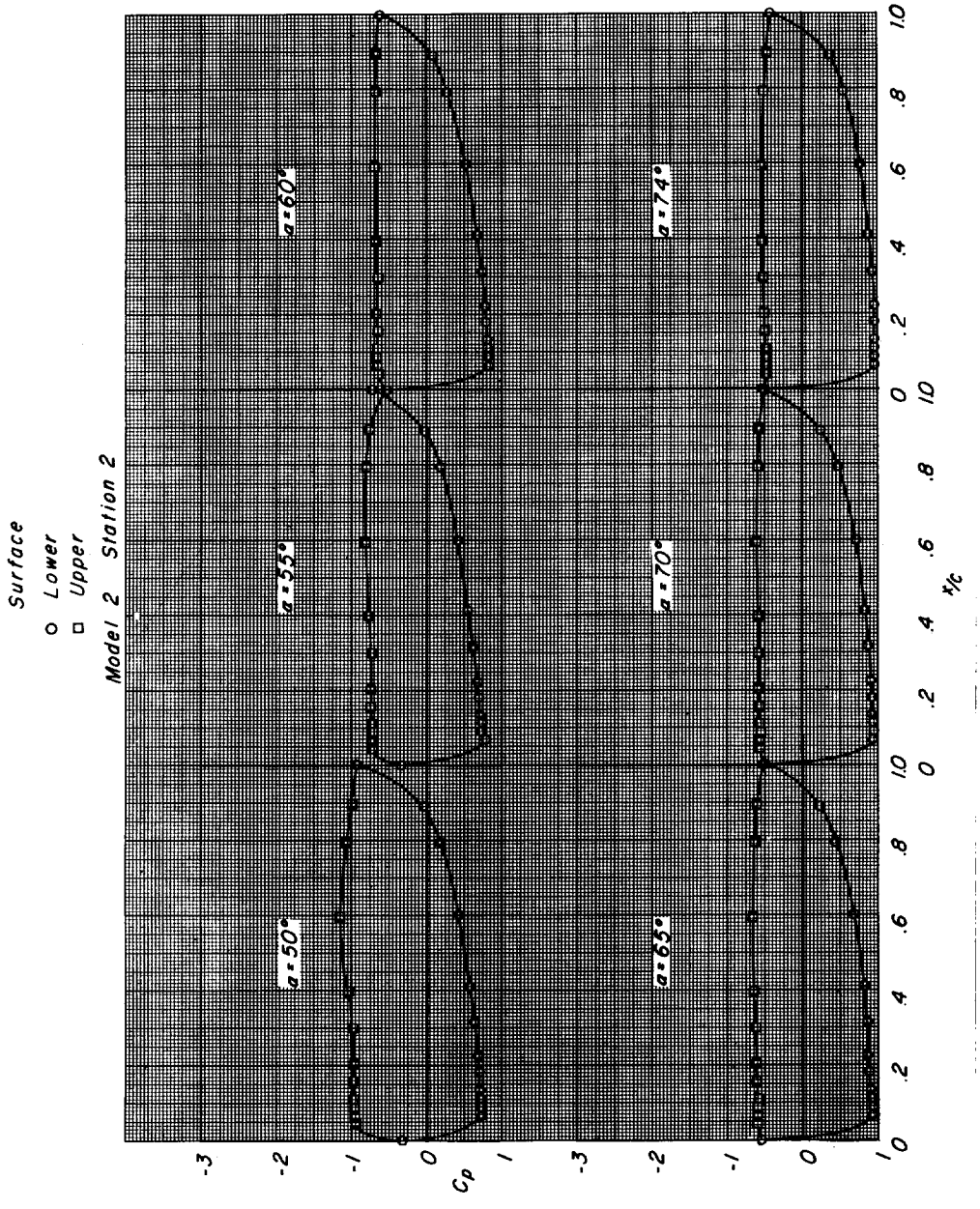

(b) Concluded.

Figure 7.- Continued.

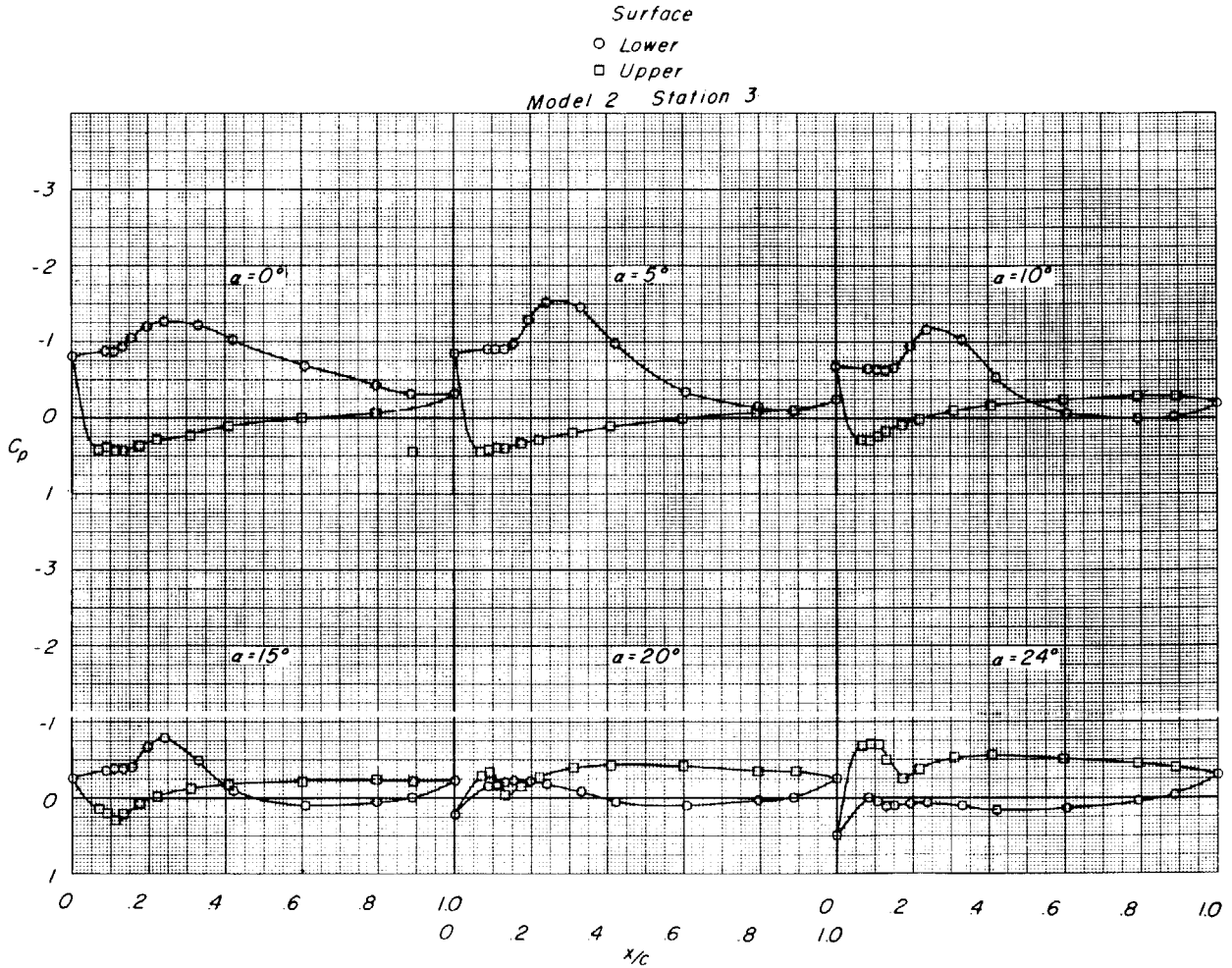

(c) Station 3.

Figure 7.- Continued.

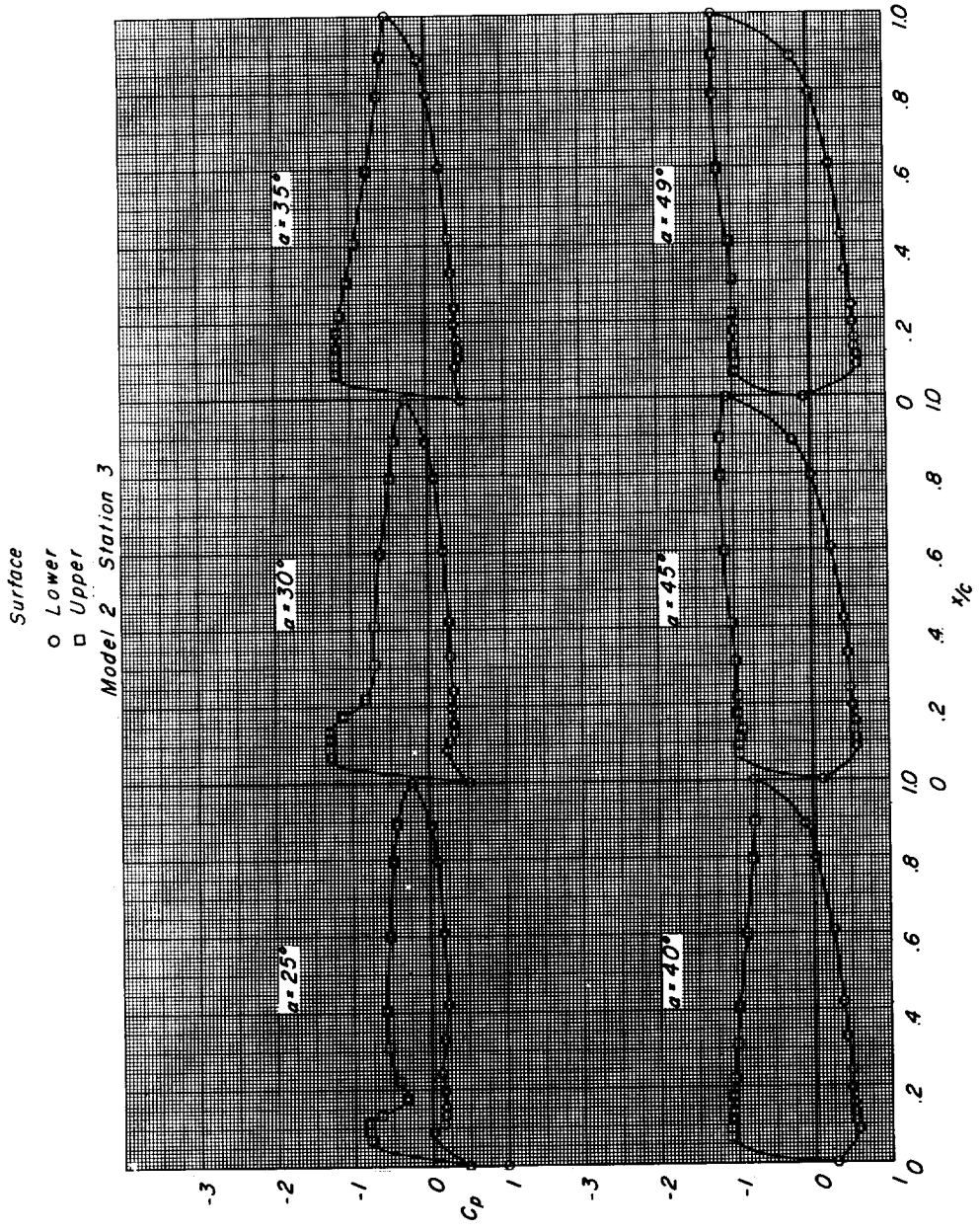

(c) Continued.

Figure 7.- Continued.

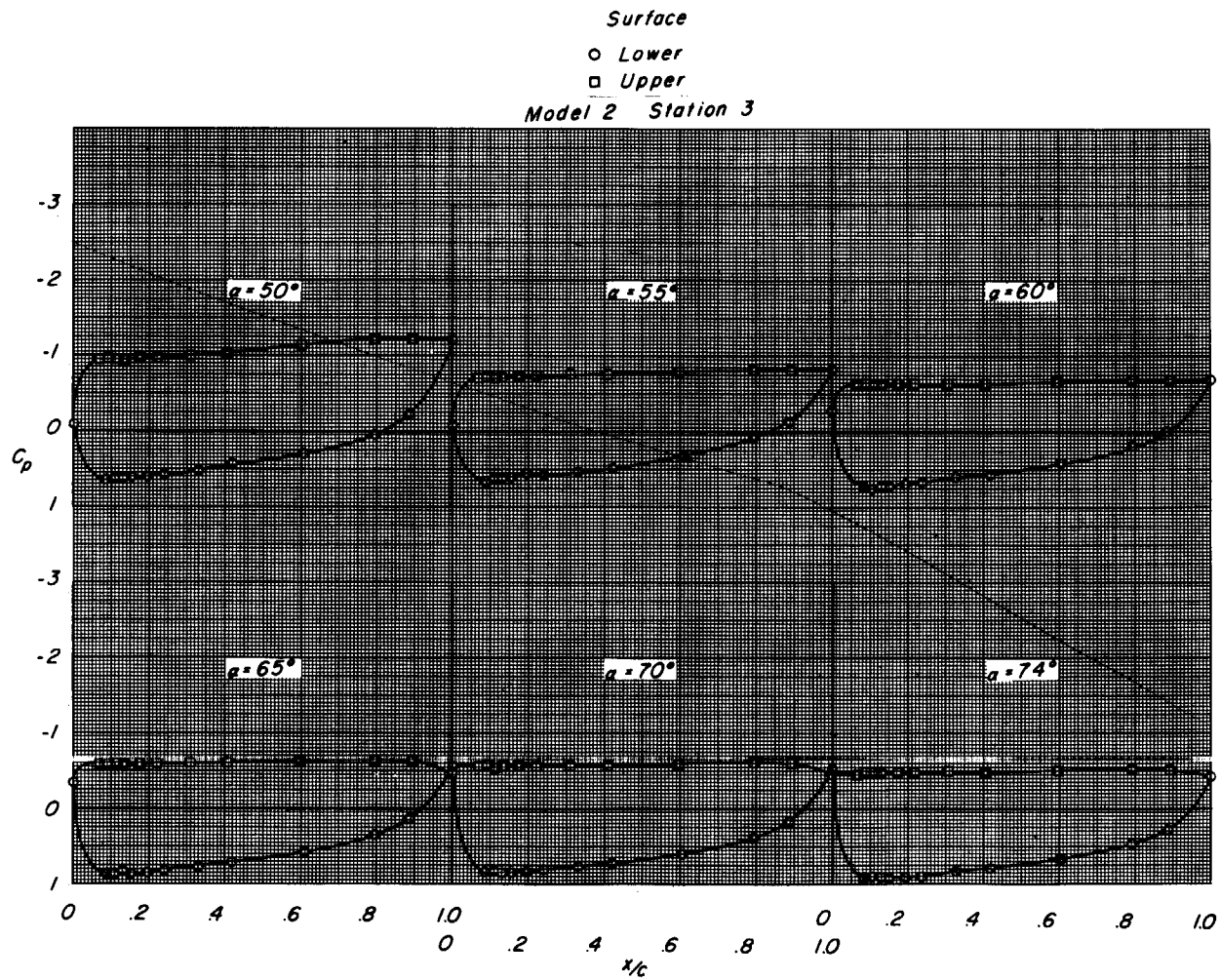

(c) Concluded.

Figure 7.- Continued.

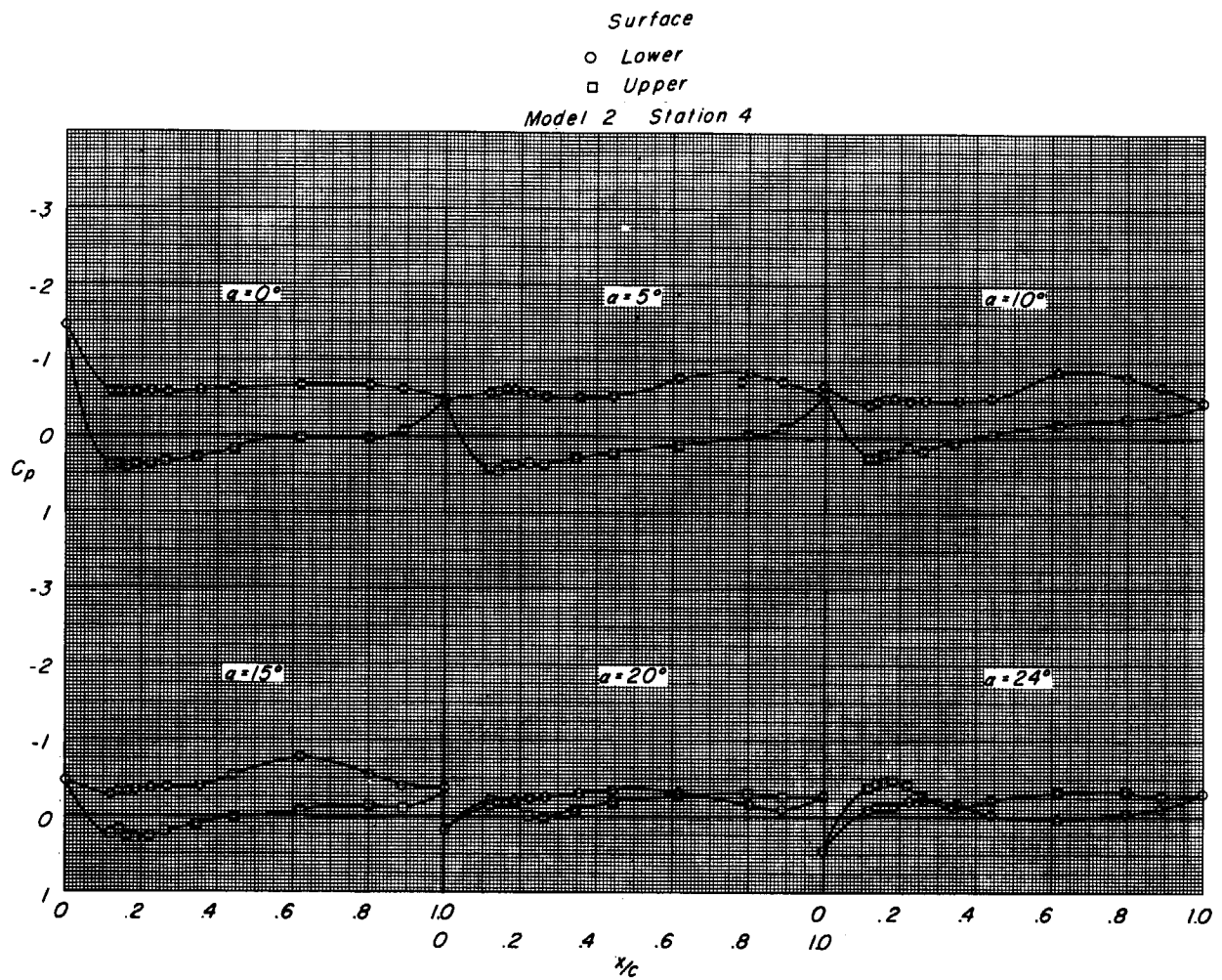

(d) Station 4.

Figure 7.- Continued.

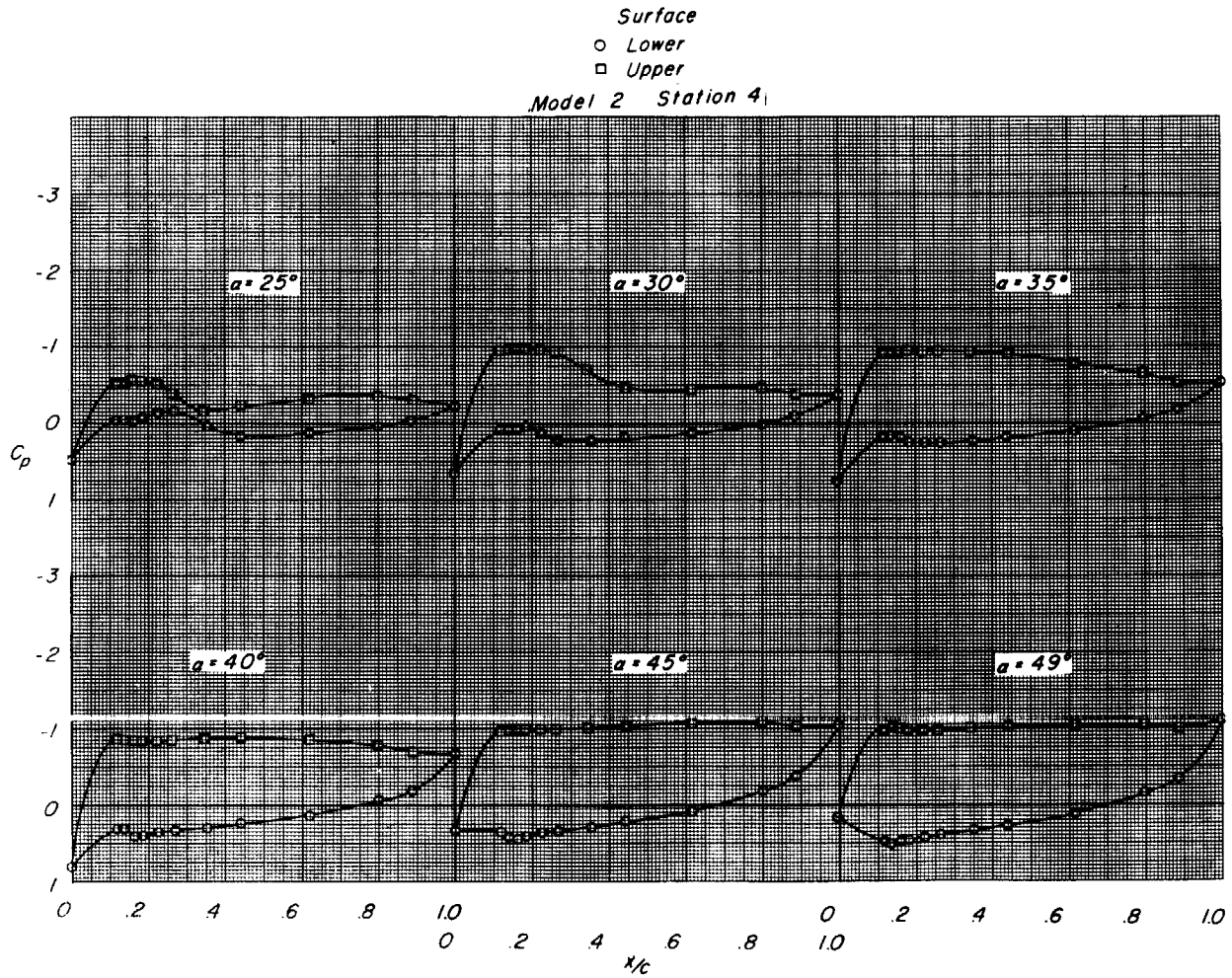

(d) Continued.

Figure 7.- Continued.

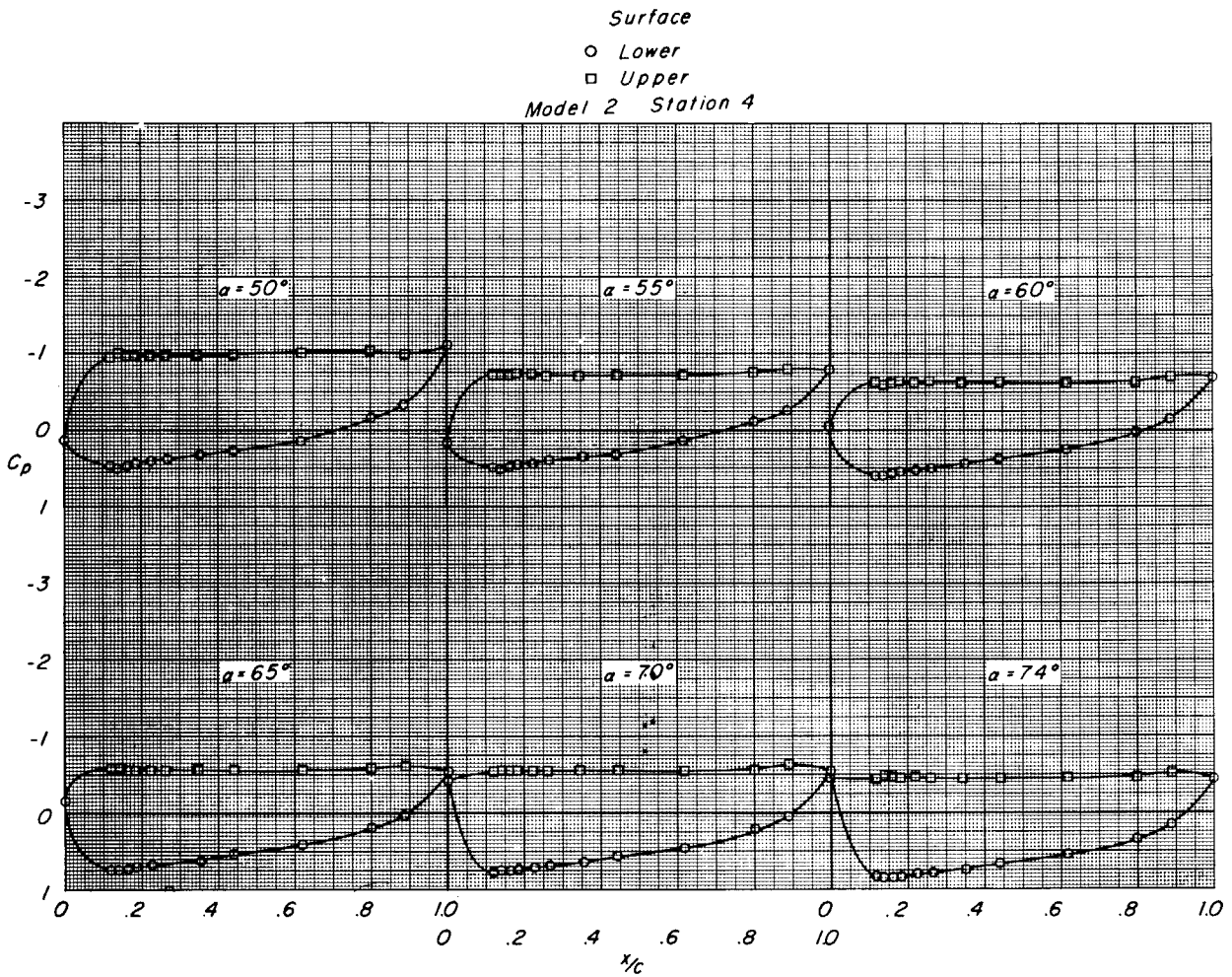

(d) Concluded.

Figure 7.- Concluded.

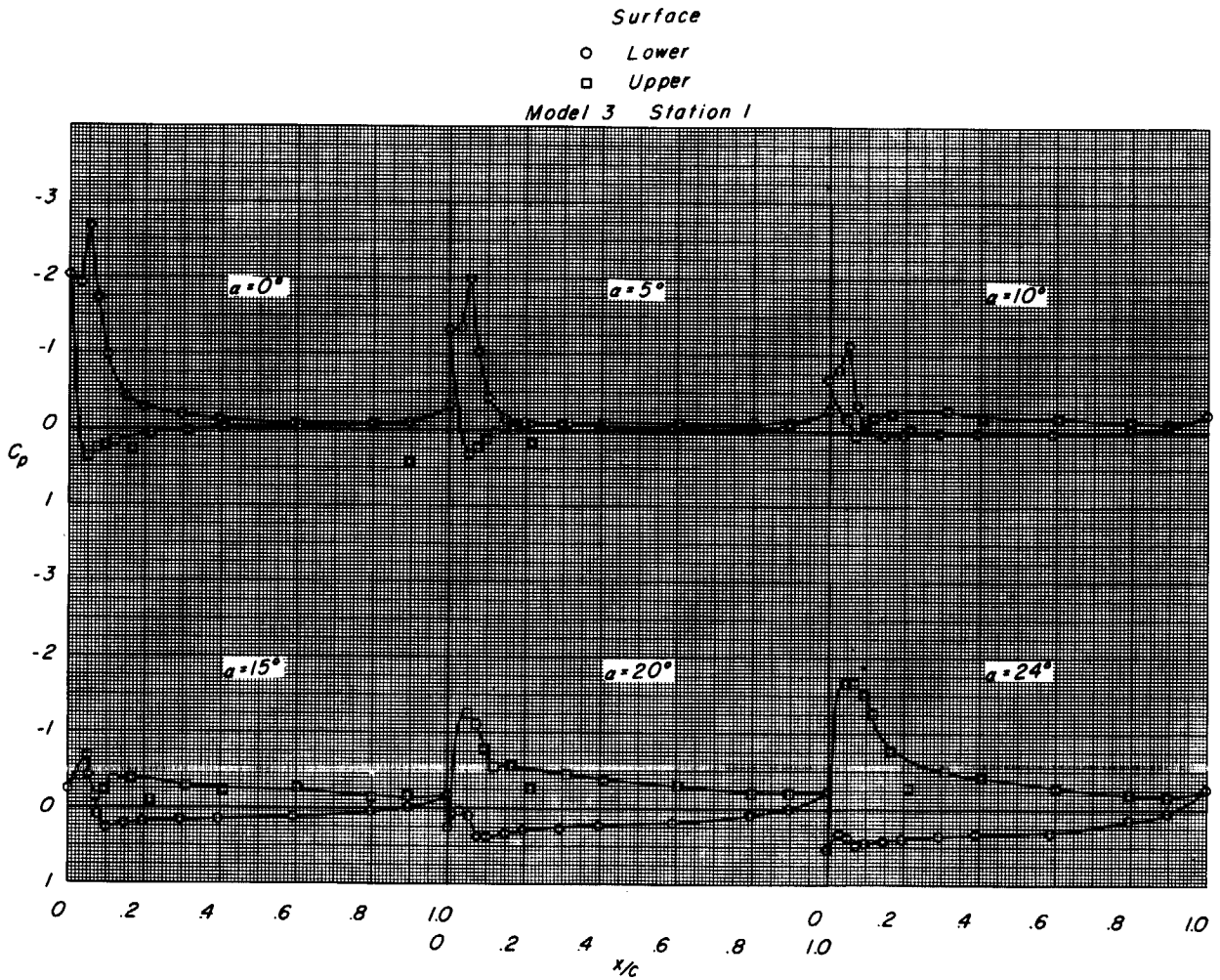

(a) Station 1.

Figure 8.- Pressure distributions on model 3 at various angles of attack.

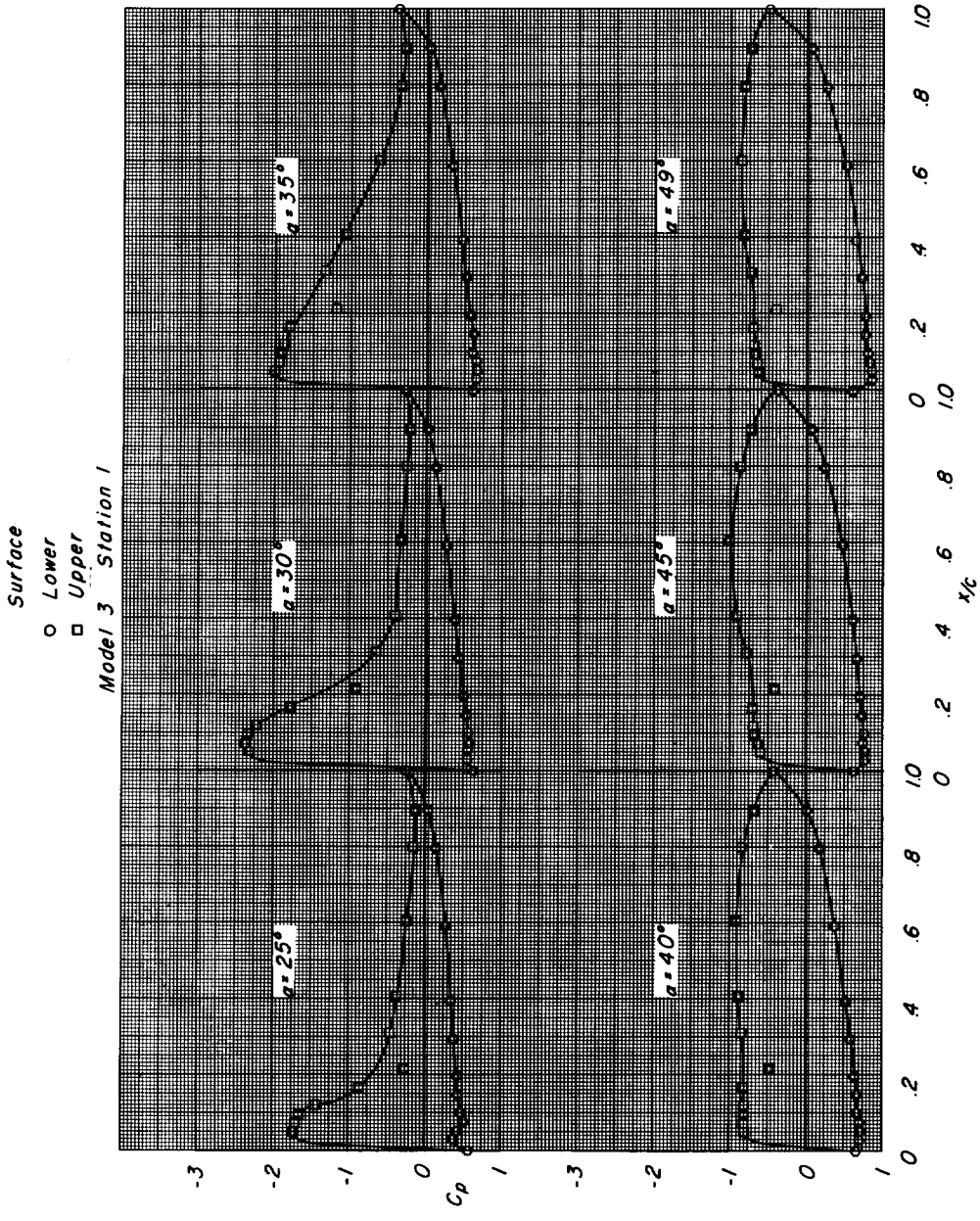

(a) Continued.

Figure 8.- Continued.

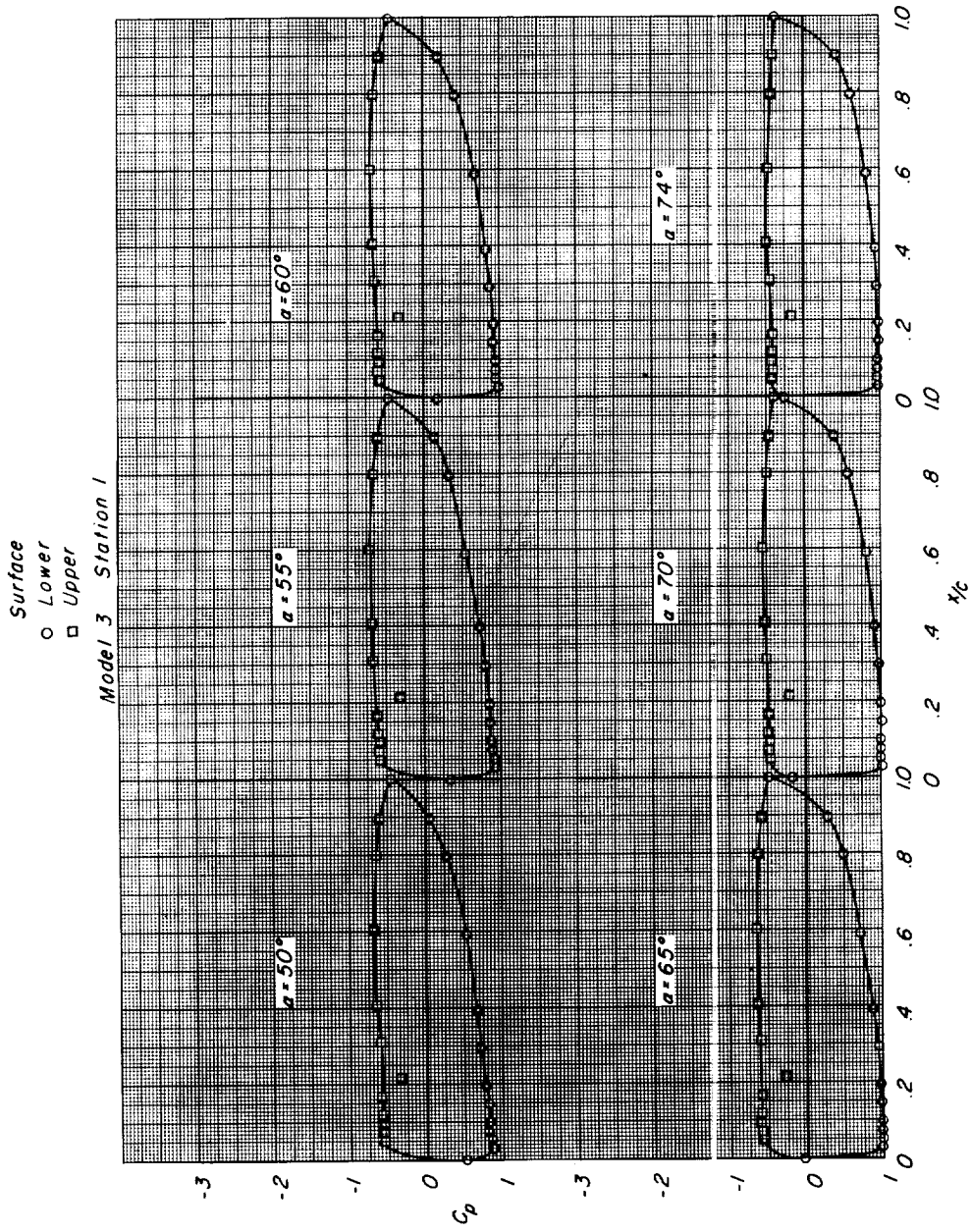

(a) Concluded.

Figure 8.- Continued.

L-1757

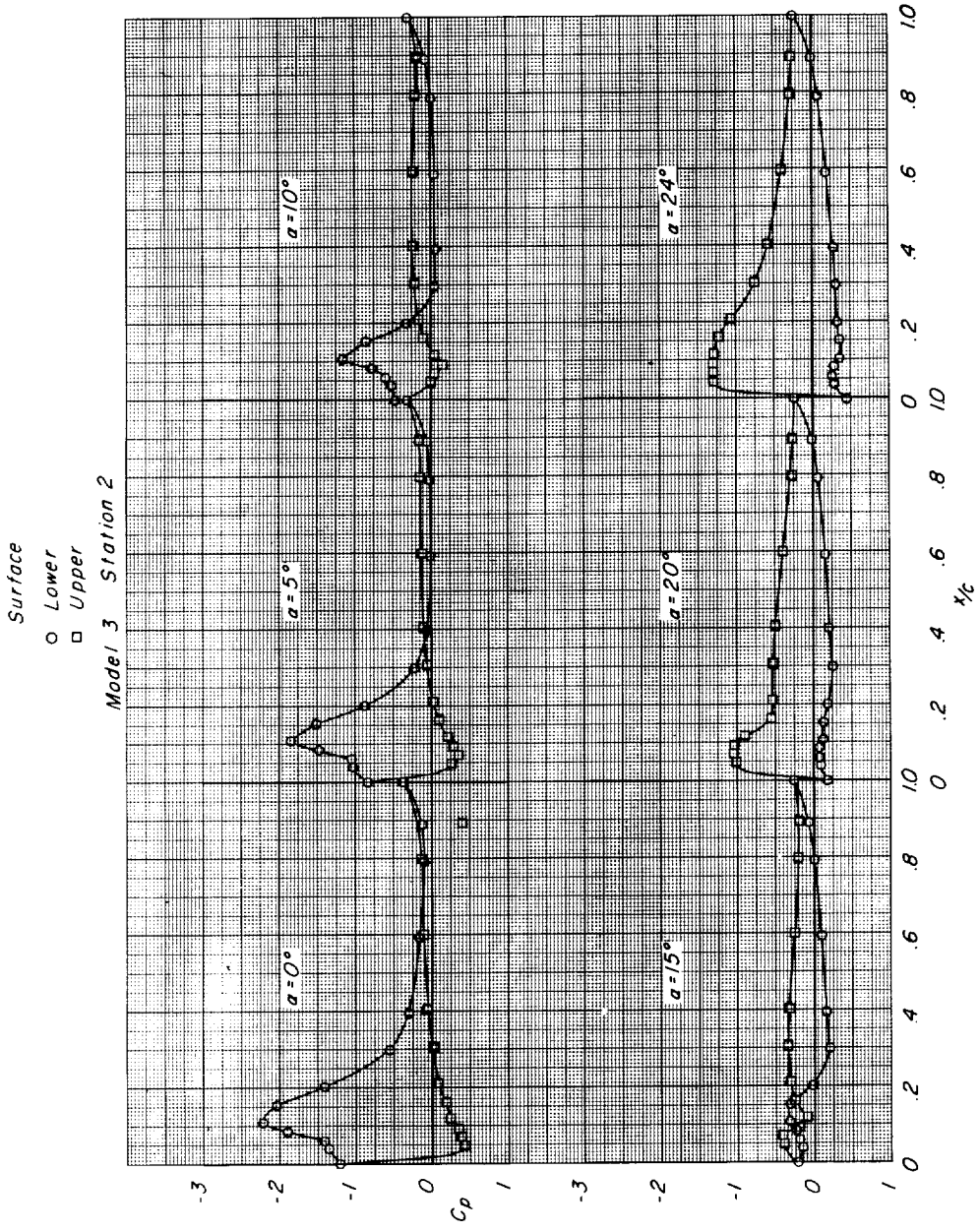

(b) Station 2.

Figure 8.- Continued.

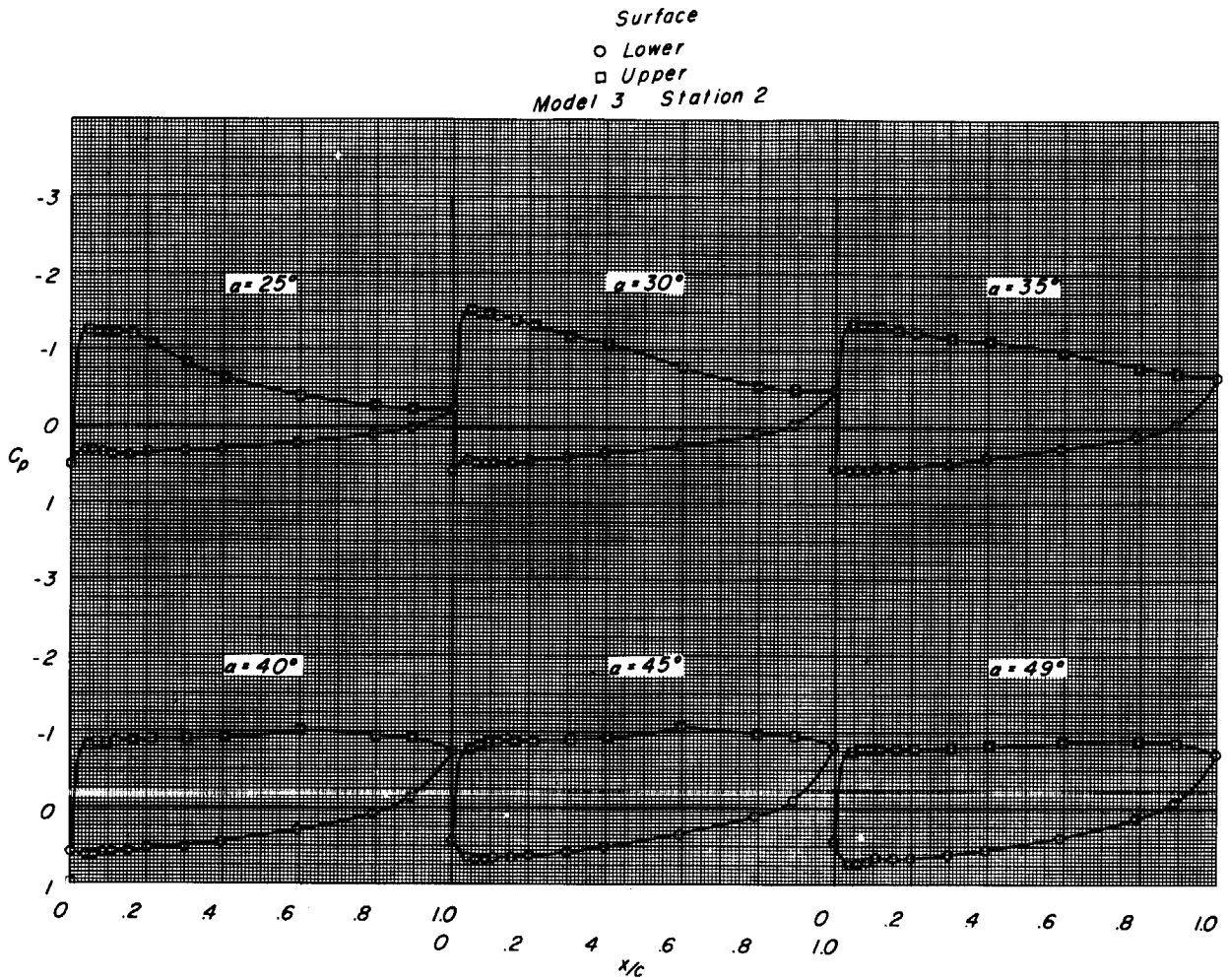

(b) Continued.

Figure 8.- Continued.

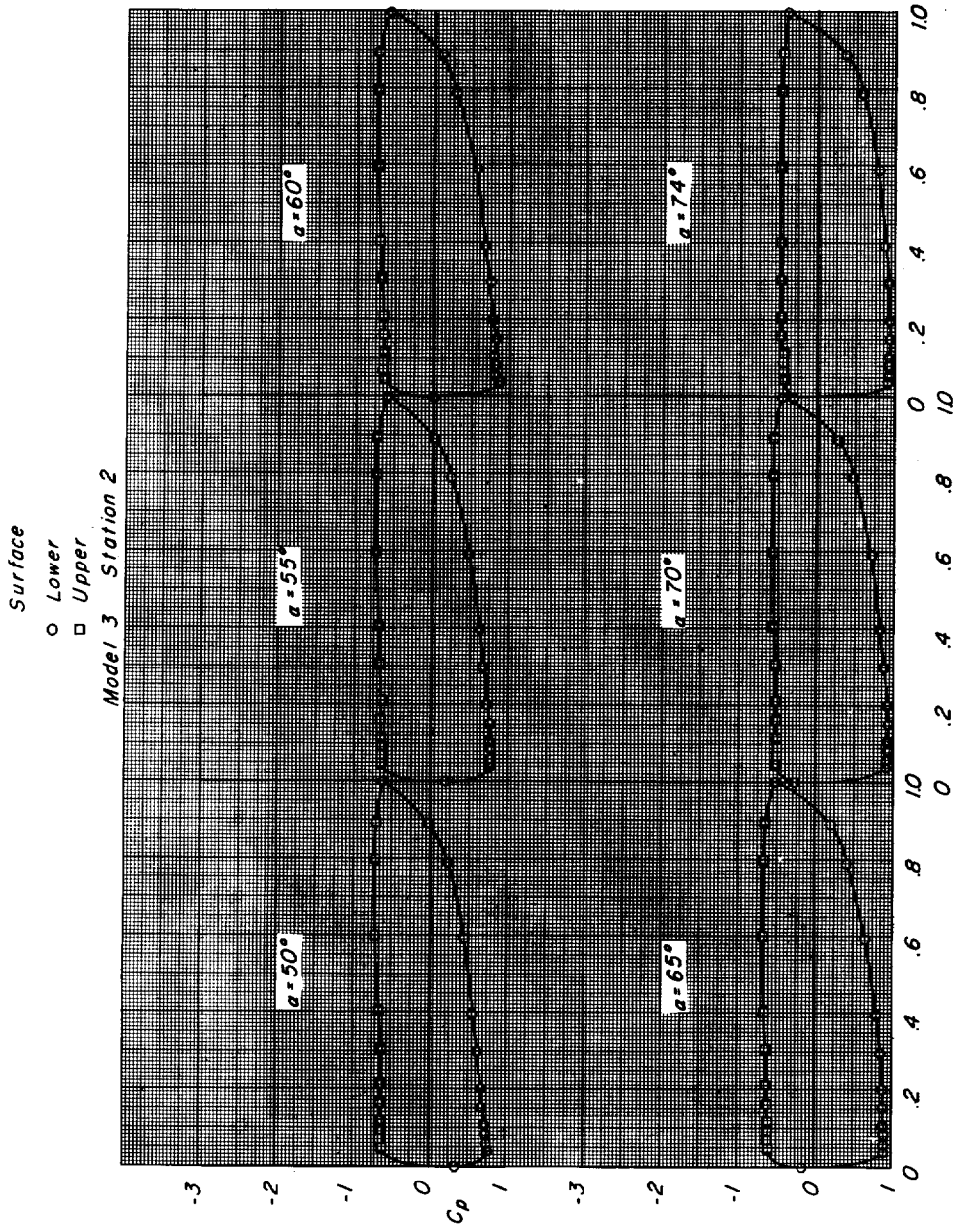

(b) Concluded.

Figure 8.- Continued.

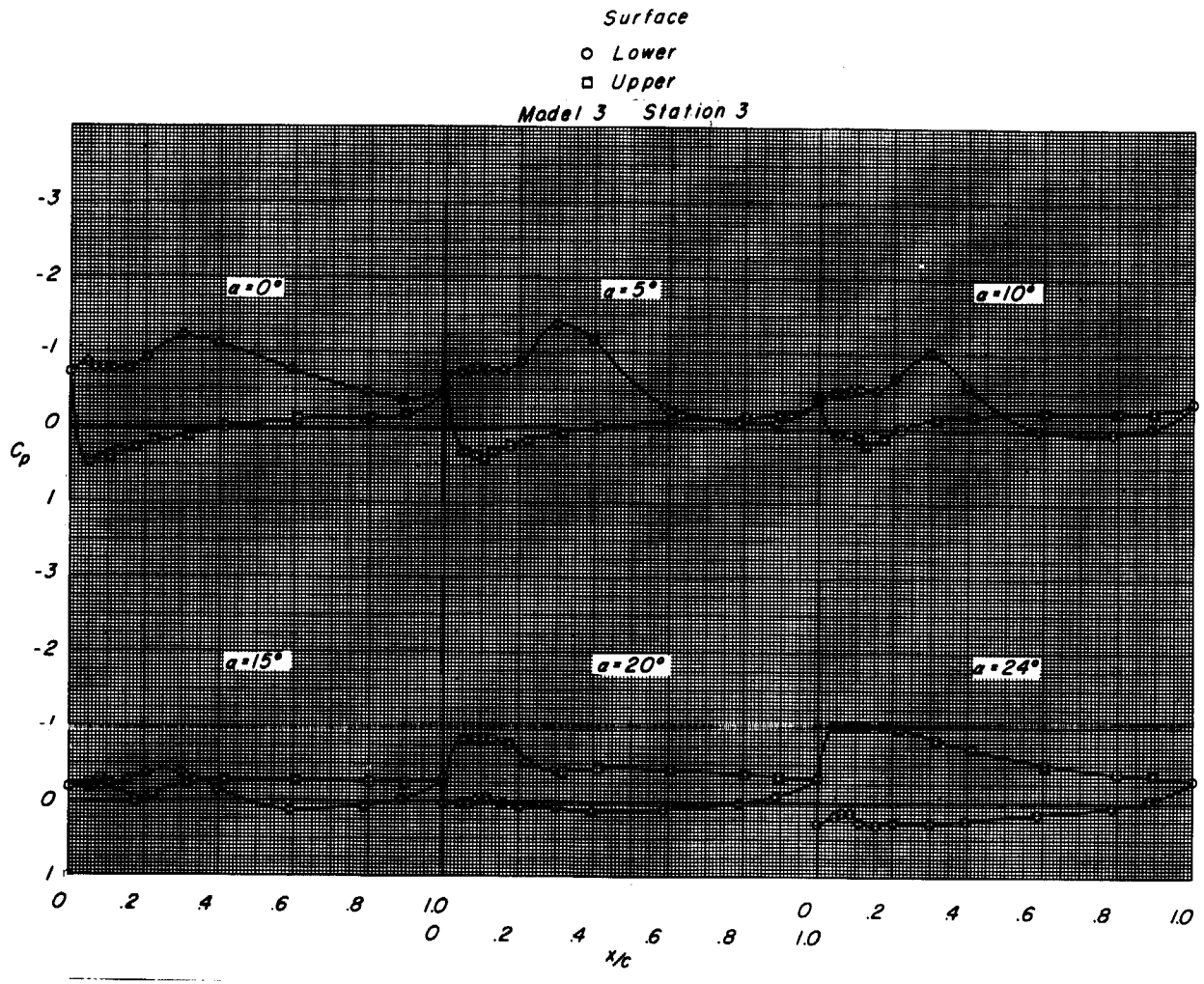

(c) Station 3.

Figure 8.- Continued.

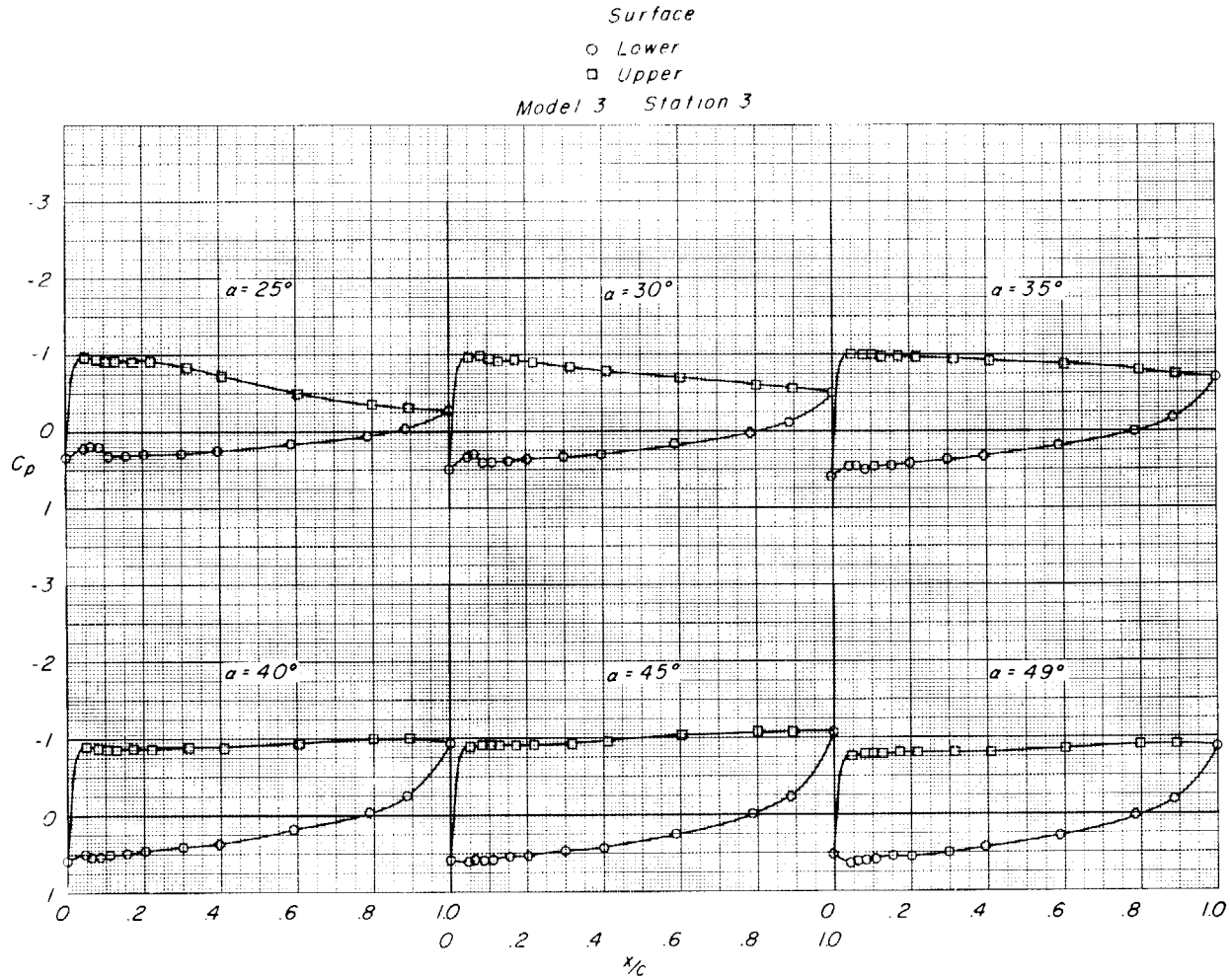

(c) Continued.

Figure 8.- Continued.

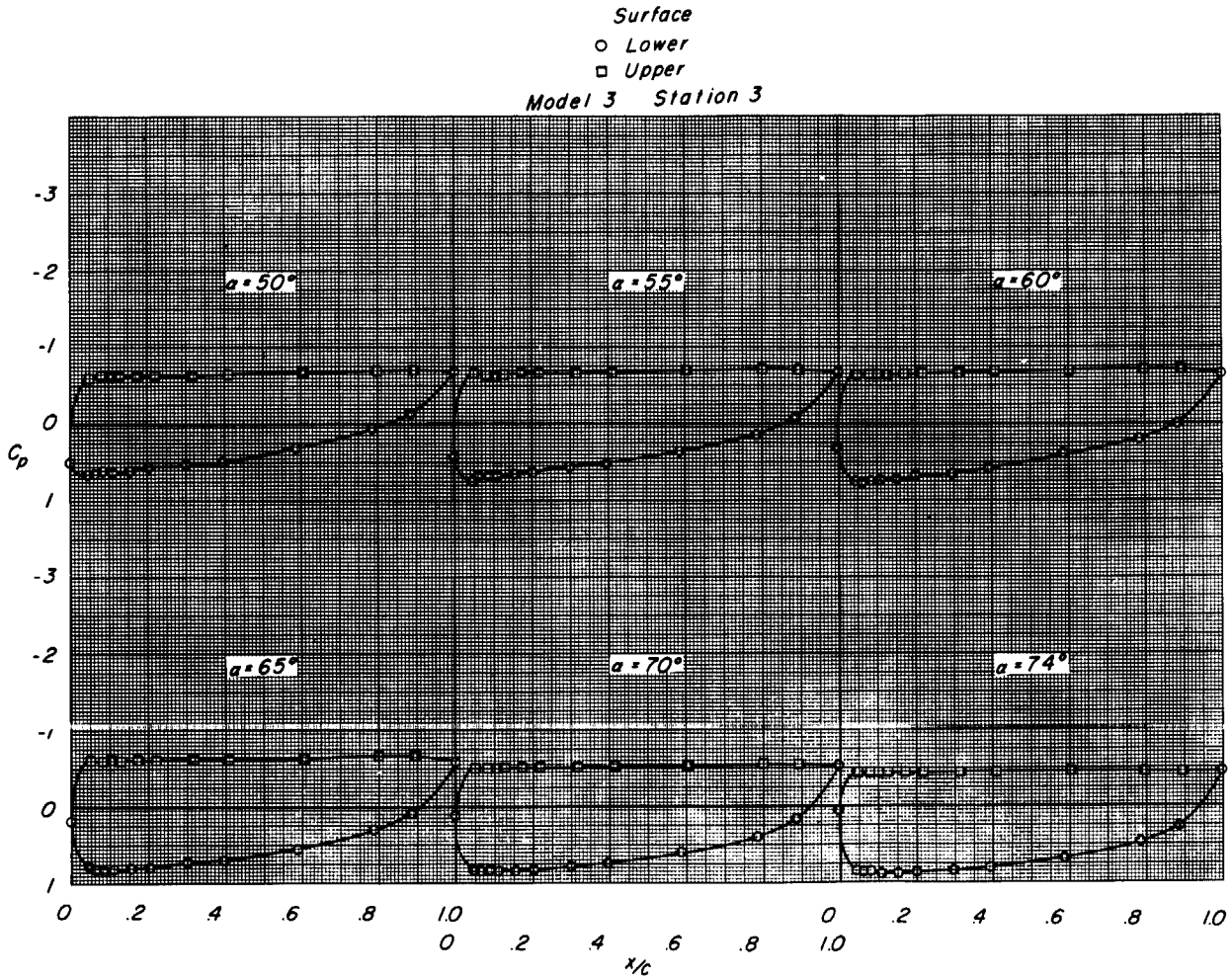

(c) Concluded.

Figure 8.- Continued.

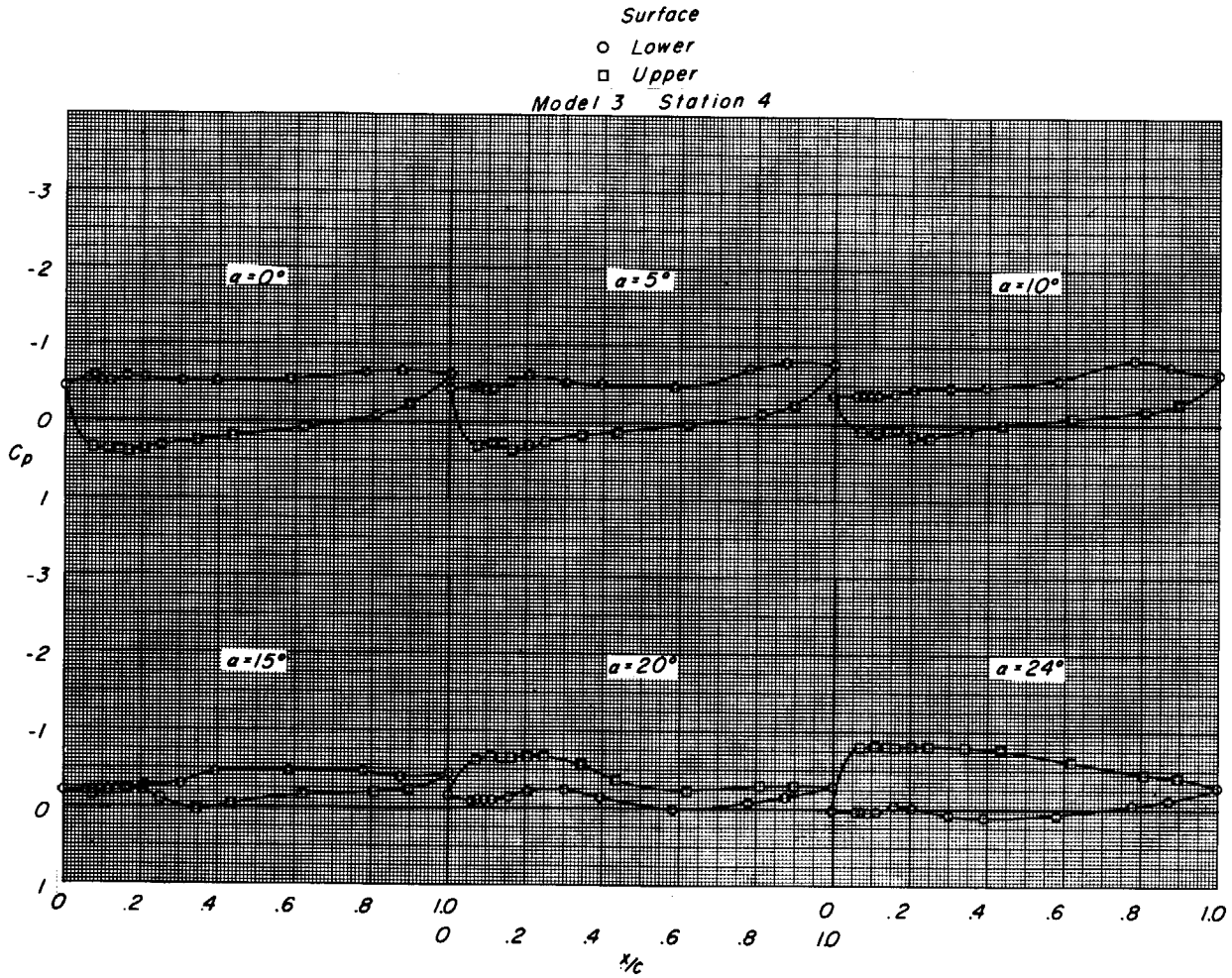

(d) Station 4.

Figure 8.- Continued.

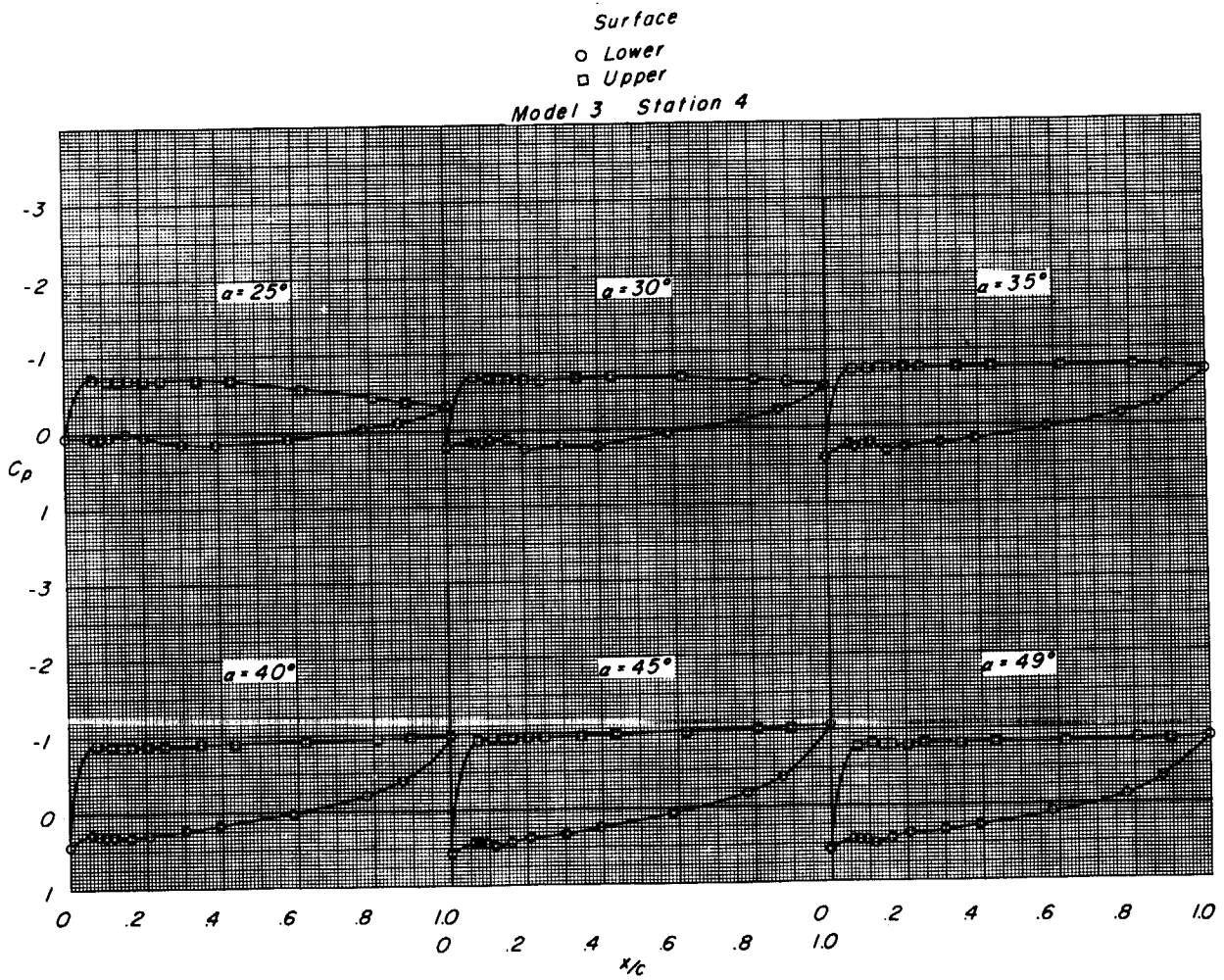

(d) Continued.

Figure 8.- Continued.

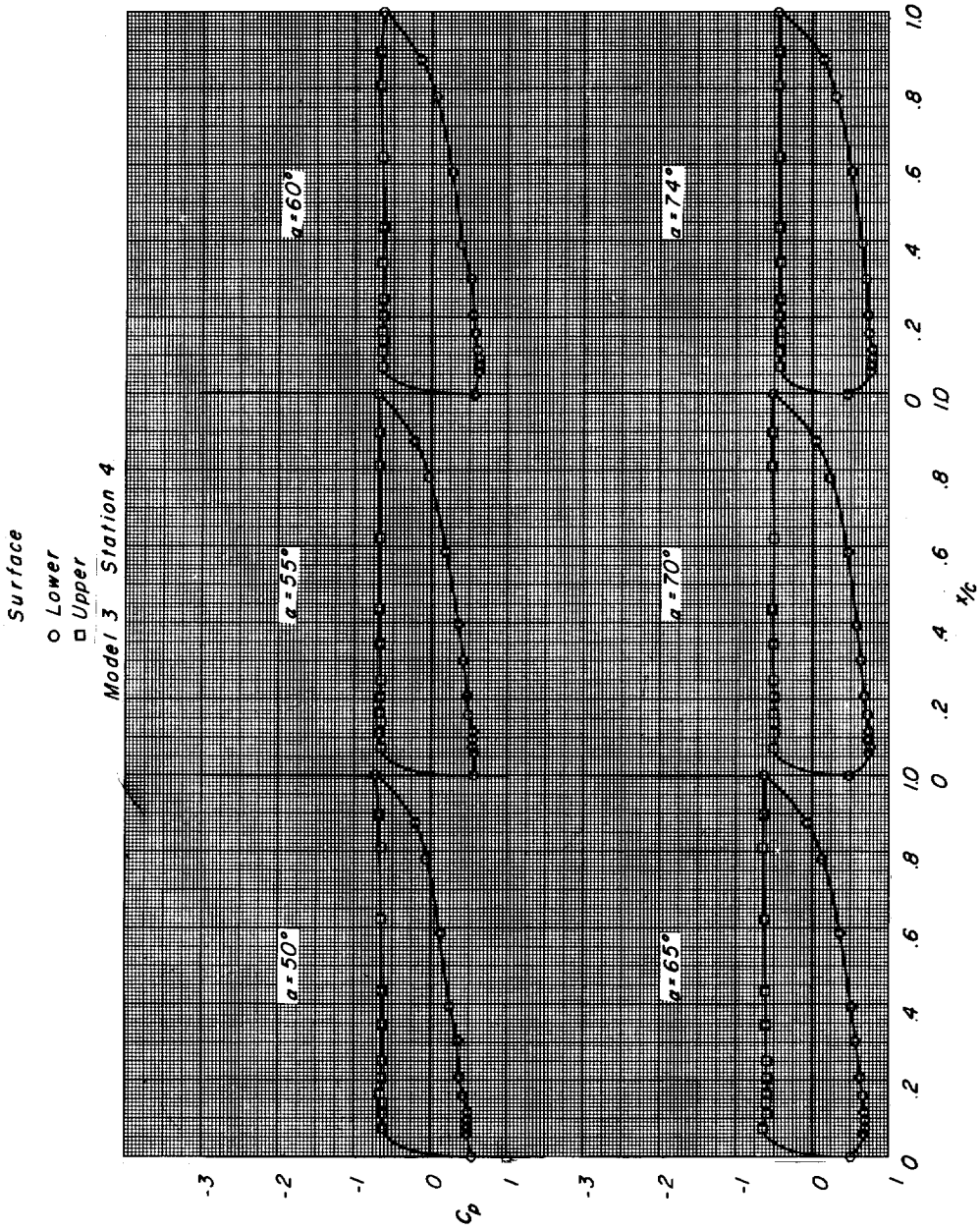

(d) Concluded.

Figure 8.- Concluded.